Chapter 2
Electric Vehicle Battery Technologies

Kwo Young, Caisheng Wang, Le Yi Wang, and Kai Strunz

2.1 Introduction

As discussed in the previous chapter, electrification is the most viable way to achieve clean and efficient transportation that is crucial to the sustainable development of the whole world. In the near future, electric vehicles (EVs) including hybrid electric vehicles (HEVs), plug-in hybrid electric vehicles (PHEVs), and pure battery electric vehicles (BEVs) will dominate the clean vehicle market [1, 2]. By 2020, it is expected that more than half of new vehicle sales will likely be EV models.[1] The key and the enabling technology to this revolutionary change is battery.

The importance of batteries to EVs has been verified in the history. The first EV was seen on the road shortly after the invention of rechargeable lead–acid batteries and electric motors in the late 1800s [4]. In the early years of 1900s, there was a golden period of EVs. At that time, the number of EVs was almost double that of gasoline power cars. However, EVs almost disappeared and gave the whole market to

[1] Though fuel cell vehicle (FCV) is one of the technologies under consideration of electric-drive vehicles, the durability, high cost, and production and distribution of hydrogen have hindered its development. The US Department of Energy (DOE) dropped its research support for FCV in its budget of fiscal year of 2010 [3].

K. Young
Ovonic Battery Company, Rochester Hills, MI, USA
e-mail: kyoung@ovonic.com

C. Wang (✉) • L.Y. Wang
Wayne State University, Detroit, MI, USA
e-mail: cwang@wayne.edu; lywang@wayne.edu

K. Strunz
Technische Universität Berlin, Berlin, Germany
e-mail: kai.strunz@tu-berlin.de

R. Garcia-Valle and J.A. Peças Lopes (eds.), *Electric Vehicle Integration into Modern Power Networks*, Power Electronics and Power Systems,
DOI 10.1007/978-1-4614-0134-6_2, © Springer Science+Business Media New York 2013

Table 2.1 Batteries used in electric vehicles of selected car manufacturers.

Company	Country	Vehicle model	Battery technology
GM	USA	Chevy-Volt	Li-ion
		Saturn Vue Hybrid	NiMH
Ford	USA	Escape, Fusion, MKZ HEV	NiMH
		Escape PHEV	Li-ion
Toyota	Japan	Prius, Lexus	NiMH
Honda	Japan	Civic, Insight	NiMH
Hyundai	South Korea	Sonata	Lithium polymer
Chrysler	USA	Chrysler 200C EV	Li-ion
BMW	Germany	X6	NiMH
		Mini E (2012)	Li-ion
BYD	China	E6	Li-ion
Daimler Benz	Germany	ML450, S400	NiMH
		Smart EV (2010)	Li-ion
Mitsubishi	Japan	iMiEV (2010)	Li-ion
Nissan	Japan	Altima	NiMH
		Leaf EV (2010)	Li-ion
Tesla	USA	Roadster (2009)	Li-ion
Think	Norway	Think EV	Li-ion, Sodium/Metal Chloride

internal combustion engine (ICE) cars by 1920 due to the limitations of heavy weight, short trip range, long charging time, and poor durability of batteries at that time.

EV batteries are quite different from those used in consumer electronic devices such as laptops and cell phones. They are required to handle high power (up to a hundred kW) and high energy capacity (up to tens of kWh) within a limited space and weight and at an affordable price. Extensive research efforts and investments have been given to the advanced battery technologies that are suitable for EVs all over the world. The U.S. government has been strongly supporting its R&D activities in advanced batteries through the Department of Energy (DOE): about $2 billion grants to accelerate the manufacturing and development of the next generation of U.S. batteries and EVs [1]. European Commission and governmental organizations in Europe and Japanese Ministry of Economy, Trade and Industry (METI) have also been continuously supporting the R&D activities in advanced batteries. BYD, Lishen, and Chunlan have obtained strong subsidy supports from the Chinese government for its research and manufacturing of advanced batteries and electric vehicles.

As shown in Table 2.1 [4], the current two major battery technologies used in EVs are nickel metal hydride (NiMH) and lithium ion (Li-ion). Nearly all HEVs available in the market today use NiMH batteries because of its mature technology. Due to the potential of obtaining higher specific energy and energy density, the adoption of Li-ion batteries is expected to grow fast in EVs, particularly in PHEVs and BEVs. It should be noted that there are several types of Li-ion batteries based on similar but certainly different chemistry.

EVs can be integrated into the power grid in future. They can be aggregated together for grid supports such as renewable accommodation, frequency regulation,

voltage profile regulation, and system optimization. They can also be operated in a distributed way and work with local loads to achieve demand side management. As to the EV grid integration issues discussed in the book, the battery inside the EVs is the key component. In this chapter, the fundamentals of EV battery technologies will be addressed. The focus will be given to the two most common EV battery technologies: NiMH and Li-ion. It is particularly important for power engineers to understand the basic chemistry of the different batteries, and specific EV battery requirements of energy density, specific energy, power density, cost, durability, etc. The EV battery modeling will be introduced in the way that it is suitable for power engineers to appreciate and use it for power electronic interfacing converter design, battery management, and system level studies. The performance of a battery changes as its operating conditions (temperature, charging or discharging current, state of charge (SOC), etc.) and its service time vary. This chapter will also cover the topic on battery characterization including battery model parameter estimation, SOC and state of health (SOH) estimation. The battery power management and the re-use of second-hand EV batteries for stationary power grid applications will be discussed at the end of this chapter.

2.2 Power and Energy of Electric Propulsion

Depending on the actual configuration of an EV, part or all of its propulsion power and energy is supplied by the battery inside the vehicle. Without loss of generality, the discussion in this subsection is for a pure battery EV. Similar to those in regular vehicles, the powertrain in an EV needs to provide power for the vehicle under all kinds of road conditions and driving modes. In addition, an EV also needs to handle regenerative braking so that the kinetic energy of the moving vehicle can be captured and stored in battery for future use.

The acceleration of a vehicle is determined by all the forces applied on it, which is given by Newton's second law as [5]

$$f_m M\alpha = F_t - \sum F_r, \tag{2.1}$$

where M is the overall mass of the vehicle, α is the vehicle acceleration, f_m is the mass factor that converts the rotational inertias of rotating components into equivalent translational mass, F_t is the total traction force to the vehicle, and $\sum F_r$ is the total resistive force. The resistive forces are normally the rolling resistance between tires and road surface, aerodynamic drag, and uphill grading resistance. The total resistance can be estimated as [5]

$$\sum F_r = MgC_{rr}\cos\theta + \frac{1}{2}\rho A C_d (V - V_w)^2 + Mg\sin\theta, \tag{2.2}$$

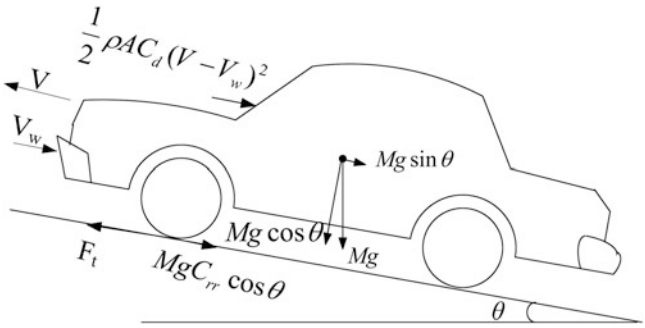

Fig. 2.1 Forces applied on a vehicle

where g is the acceleration of gravity, C_{rr} is coefficient of rolling resistance between tires and road surface, ρ is the density of the ambient air, A is the vehicle frontal area, C_d is the aerodynamic drag coefficient, V is the vehicle speed, V_w is the wind speed in the vehicle moving direction, and θ is the slope angle. For a downhill slope, θ will have a negative value (Fig. 2.1).

The total propulsion force can then be expressed as

$$F_t = f_m M\alpha + MgC_{rr}\cos\theta + \frac{1}{2}\rho AC_d(V - V_w)^2 + Mg\sin\theta. \tag{2.3}$$

The power to drive the vehicle at speed V is then

$$P = F_t V = f_m M\alpha V + MgC_{rr}V\cos\theta + \frac{1}{2}\rho AC_d V(V - V_w)^2 + MgV\sin\theta. \tag{2.4}$$

For a vehicle on a flat road ($\theta = 0$), at the early stage of acceleration, the propulsion power is mainly used to accelerate the vehicle and to overcome the rolling resistance. When the speed is reached, the power is used to keep the speed by overcoming the rolling resistance and aerodynamic drag force. For an electric vehicle, the battery power capability needs to be sufficient to meet acceleration requirements. For accelerating a vehicle with the parameters listed in Table 2.2, according to (2.4), it needs about 61 kW on average to accelerate the vehicle to 96.6 km/h (or 60 mph) in 10 s.

In the procedure of regenerative braking, the electric propulsion motor in an EV works as a generator to convert the kinetic energy of vehicle motion into electrical energy and charge battery. The braking power can be expressed as

$$P_b = F_b V = f_m M\mu V - MgC_{rr}V\cos\theta - \frac{1}{2}\rho AC_d V(V - V_w)^2 - MgV\sin\theta, \tag{2.5}$$

where P_b is the braking power, F_b is the braking force, and μ is the deceleration of the vehicle.

Table 2.2 Propulsion power of a typical vehicle.

Mass	1,360 kg
Mass factor, f_m	1.05
Acceleration, 0 to 96.6 km/h in 10 s	2.68 m^2/s
Coefficient of rolling resistance	0.02
Air density	1.225 kg/m^3
Vehicle frontal area	2 m^2
Aerodynamic drag coefficient	0.5
Wind speed	0 m/s
Road slope angle	0°
Average power during the acceleration	60.8 kW

For the same vehicle listed in Table 2.2, the peak braking power for bringing the vehicle moving at 96.6 km/h to stop in 5 s can be as high as 186 kW. It can be seen that the power rating requirement is higher for braking since the de-acceleration may have to happen in a shorter period of time. The battery in the electric powertrain is required to meet the demands from both supplying and absorbing the high power.

A more challenging issue to EV is the energy capability of battery. According to the U.S. urban dynamometer driving schedule (UDDS) and the highway fuel economy driving schedule (HWFEDS) also called the highway fuel economy test (HWFET), typical energy consumption of a mid-size vehicle for urban driving is 165 Wh/km and 137 Wh/kg for highway. There are more aggressive driving schedules such as US 06 with an energy consumption close to 249 Wh/km [4]. Using the weighting factors of 45% urban, 45% highway, and 10% US 06, we can then get an average energy consumption rate of 160 Wh/kg (45% × 137 Wh/km + 45% × 165 Wh/km + 10% × 249 Wh/kg). Though the energy consumption during driving depends on many factors such as vehicle size, weight, body shape, and the driving habit of the driver, the key factor is the capacity of the energy storage device. The high value of specific energy of gasoline gives a conventional ICE powered vehicle a range of 300–400 miles with a full tank of gasoline. Gasoline has a theoretical specific energy of 13,000 Wh/kg, which is over 100 times higher than the specific energy of 120 Wh/kg of typical Li-ion batteries. It would be too big and heavy to have a battery pack with the same amount of energy as a full tank (e.g., 16 gallons) of gasoline. However, since the electric propulsion is much more efficient than an ICE, less energy is needed to propel an EV. Considering the efficiency of 80% for EV propulsion and 20% for ICE, the total amount of energy stored for EV can be a quarter of what a regular ICE powered vehicle needs for the same mileage. Based on the current battery technology, it is not practical to consider a pure BEV with a mile range of 300–400 miles since it would require a battery pack larger than 100 kWh that can weigh over 900 kg. Nevertheless, it is realistic to have a battery pack around 30 kWh to achieve 100 mile range even based on current battery technologies.

2.3 Basic Terms of Battery Performance and Characterization

Various terms have been defined for batteries to characterize their performance. Commonly used terms are summarized in the following as a quick reference.

Cell, Module, and Pack. A single cell is a complete battery with two current leads and separate compartment holding electrodes, separator, and electrolyte. A module is composed of a few cells either by physical attachment or by welding in between cells. A pack of batteries is composed of modules and placed in a single containing for thermal management. An EV may have more than one pack of battery situated in a different location in the car.

Ampere-hour Capacity. Ampere-hour (Ah) capacity is the total charge that can be discharged from a fully charged battery under specified conditions. The *Rated Ah capacity* is the nominal capacity of a fully charged new battery under the conditions predefined by the manufacturer. A nominal condition, for example, can be defined as 20°C and discharging at 1/20 C-rate. People also use Wh (or kWh) capacity to represent a battery capacity. The rated Wh capacity is defined as

$$Rated\ Wh\ Capacity = Rated\ Ah\ Capacity \times Rated\ Battery\ Voltage. \tag{2.6}$$

C-rate. C (*nominal C-rate*) is used to represent a charge or discharge rate equal to the capacity of a battery in one hour. For a 1.6 Ah battery, *C* is equal to charge or discharge the battery at 1.6 A. Correspondingly, *0.1C* is equivalent to 0.16 A, and *2C* for charging or discharging the battery at 3.2 A.

Specific Energy. Specific energy, also called gravimetric energy density, is used to define how much energy a battery can store per unit mass. It is expressed in Watt-hours per kilogram (Wh/kg) as

$$Specific\ Energy = Rated\ Wh\ Capacity/Battery\ Mass\ in\ kg. \tag{2.7}$$

Specific energy of a battery is the key parameter for determining the total battery weight for a given mile range of EV.

Specific Power. Specific power, also called gravimetric power density of a battery, is the peak power per unit mass. It is expressed in W/kg as

$$Specific\ Power = Rated\ Peak\ Power/Battery\ Mass\ in\ kg. \tag{2.8}$$

Energy Density. Energy density, also referred as the volumetric energy density, is the nominal battery energy per unit volume (Wh/l).

Power Density. Power density is the peak power per unit volume of a battery (W/l).

Internal Resistance. Internal resistance is the overall equivalent resistance within the battery. It is different for charging and discharging and may vary as the operating condition changes.

Peak Power. According to the U.S. Advanced Battery Consortium (USABC)'s definition, the peak power is defined as [6]

$$P = \frac{2V_{oc}^2}{9R}, \tag{2.9}$$

where V_{oc} is the open-circuit voltage and R is the internal resistance of battery. The peak power is actually defined at the condition when the terminal voltage is 2/3 of the open-circuit voltage.

Cut-off Voltage. Cut-off voltage is the minimum allowable voltage defined by the manufacturer. It can be interpreted as the "empty" state of the battery.

State of Charge (SOC). SOC is defined as the remaining capacity of a battery and it is affected by its operating conditions such as load current and temperature.

$$SOC = \frac{Remaining\,Capacity}{Rated\,Capacity}. \tag{2.10}$$

If the Ah capacity is used, the change of SOC can be expressed as

$$\Delta SOC = SOC(t) - SOC(t_0) = \frac{1}{Ah\,Capacity}\int_{t0}^{t} i(\tau)d\tau. \tag{2.11}$$

SOC is a critical condition parameter for battery management. Accurate gauging of SOC is very challenging, but the key to the healthy and safe operation of batteries.

Depth of Discharge (DOD). DOD is used to indicate the percentage of the total battery capacity that has been discharged. For deep-cycle batteries, they can be discharged to 80% or higher of DOD.

$$DOD = 1 - SOC. \tag{2.12}$$

State of Health (SOH). SOH can be defined as the ratio of the maximum charge capacity of an aged battery to the maximum charge capacity when the battery was new [7]. SOH is an important parameter for indicating the degree of performance degradation of a battery and for estimating the battery remaining lifetime.

$$SOH = \frac{Aged\,Energy\,Capacity}{Rated\,Energy\,Capacity}. \tag{2.13}$$

Cycle Life (number of cycles). Cycle life is the number of discharge–charge cycles the battery can handle at a specific DOD (normally 80%) before it fails to meet specific performance criteria. The actual operating life of the battery is affected by the charging and discharging rates, DOD, and other conditions such as temperature.

The higher the DOD, the shorter the cycle life. To achieve a higher cycle life, a larger battery can be used for a lower DOD during normal operations.

Calendar Life. Calendar life is the expected life span of the battery under storage or periodic cycling conditions. It can be strongly related to the temperature and SOC during storage.

Battery Reversal. Battery reversal happens when the battery is forced to operate under the negative voltage (voltage of positive electrode is lower than that in the negative electrode). It can happen on a relatively weak cell in a serially connected battery string. As the usable capacity of that particular weak cell runs out, the rest of batteries in the same string will still continue to supply the current and force the weak cell to reverse its voltage. The consequence of battery reversal is either a shortening cycle life or a complete failure.

Battery Management System (BMS). BMS is a combination of sensors, controller, communication, and computation hardware with software algorithms designed to decide the maximum charge/discharge current and duration from the estimation of SOC and SOH of the battery pack.

Thermal Management System (TMS). TMS is designed to protect the battery pack from overheating and to extend its calendar life. Simple forced-air cooling TMS is adopted for the NiMH battery, while more sophisticated and powerful liquid-cooling is required by most of the Li-ion batteries in EV applications.

2.4 Battery Charging Methods and EV Charging Schemes

The safety, durability, and performance of batteries are highly dependent on how they are charged or discharged. Abuse of a battery can significantly reduce its life and can be dangerous. A current BMS includes both charging and discharging control on-board. In the future, it will be integrated into the grid energy distribution system. Hence, the focus here is given to the discussion on battery charging and charging infrastructure of EVs.

2.4.1 Charging Methods

For EV batteries, there are the following common charging methods [8]:

1. Constant Voltage. Constant voltage method charges battery at a constant voltage. This method is suitable for all kinds of batteries and probably the simplest charging scheme. The battery charging current varies along the charging process. The charging current can be large at the initial stage and gradually decreases to zero when the battery is fully charged. The drawback in this method

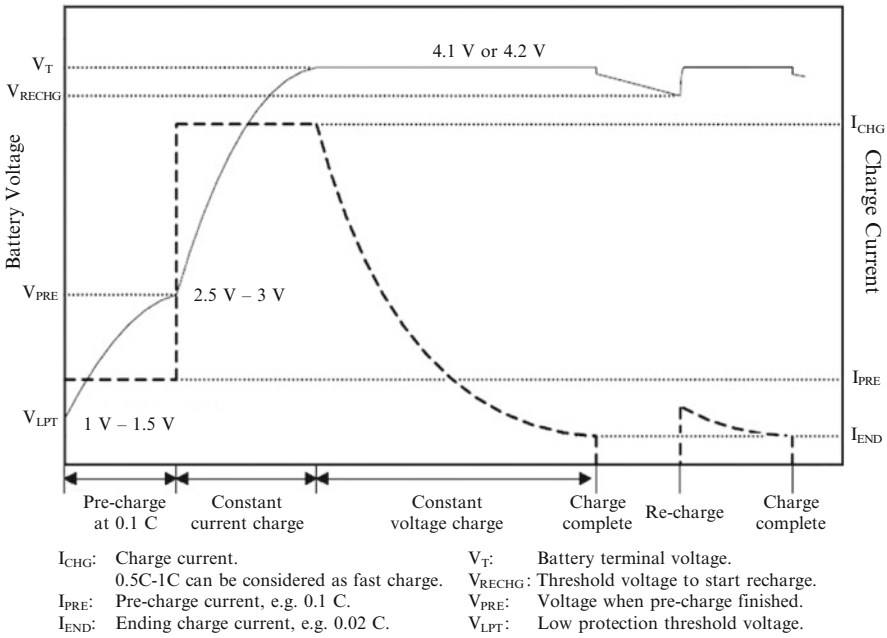

Fig. 2.2 Typical Li-ion cell charge profile

is the requirement of very high power in the early stage of charging, which is not available for most residential and parking structures.

2. Constant Current. In this charging scheme, the charging voltage applied to the battery is controlled to maintain a constant current to the battery. The SOC will increase linearly versus time for a constant current method. The challenge of this method is how to determine the completeness of a charge with SOC = 100%. The cut-off can be determined by the combination of temperature raise, temperature gradient raise, voltage increase, minus voltage change, and charging time.
3. The combination of constant voltage and constant current methods. During the charging process of a battery, normally both the methods will be used. Figure 2.2 shows a charging profile of a Li-ion cell. At the initial stage, the battery can be pre-charged at a low, constant current if the cell is not pre-charged before. Then, it is switched to charge the battery with constant current at a higher value. When the battery voltage (or SOC) reaches a certain threshold point, the charging is changed to constant voltage charge. Constant voltage charge can be used to maintain the battery voltage afterward if the DC charging supply is still available.

For EVs, it is important for batteries to be able to handle random charging due to regenerative braking. As discussed in the previous section, the braking power of regenerative braking can be at the level of hundred kilowatts. Safety limitation has to be applied to guarantee the safe operation of batteries. Mechanical braking is usually used to aid regenerative braking in EVs as a supplementary and safe measure.

It is also critical to know when to stop charging a battery. It would be ideal if the battery SOC can be accurately gauged so that we can stop charging a battery when SOC reaches a preset value (e.g., 100%). As discussed later in the chapter, it has been a very challenging task to accurately estimate SOC. Even if the SOC of a battery can be exactly identified, it is also needed to have some other backup methods to stop charging. The following are some typical methods currently used to stop a charging process.

1. Timer. It is the most typical stopping method, which can be used for any types of battery. When a preset timer expires, the charging process is stopped.
2. Temperature Cut Off (TCO) . The charging will be stopped if the absolute temperature of battery rises to a threshold value.
3. Delta Temperature Cut Off (DTCO). When the delta change in battery temperature exceeds the safety value, the charging will be terminated.
4. Temperature change rate dT/dt. If the temperature change rate is over the safety threshold value, the charging process will be terminated.
5. Minimum Current (I_{min}). When the charging current reaches the lowest limit I_{min}, the charging process stops. This method is normally incorporated with a constant voltage charging scheme.
6. Voltage Limit. When the battery voltage reaches a threshold value, the charging process will be terminated. This method normally goes together with a constant current charging method.
7. Voltage Change Rate, dV/dt. The charging process stops if the battery voltage does not change versus time, or even if it starts to drop (a negative value of dV/dt).
8. Voltage Drop ($-\Delta V$). In NiMH battery, upon completion of the charge process (SOC = 100%), the temperature of the cell starts to increase due to the recombination of hydrogen and hydroxide ions and causes the cell voltage to drop. The charging will be terminated if a preset value of the voltage drop is reached.

2.4.2 EV Charging Schemes

The success of EVs will be highly dependent on whether charging stations can be built for easy access. This is also critical for the potential grid supports that EVs can provide. The first place considered for charging stations should be homes and workplaces. Other potential locations with high populations include gas stations, shopping centers, restaurants, entertaining places, highway rest areas, municipal facilities, and schools.

There have been various standards regarding the energy transfer, connection interface and communication for EV charging [8, 9]. Table 2.3 summarizes some of the standards, as also shown in Fig. 2.3. Since it is a very dynamic area, these standards may be either updated with new revisions or replaced by new standards in the near future.

Table 2.3 Standards related to electric vehicle charging

Standard	Title/description
National Electric Code Article 625	Electric Vehicle Charging System
SAE J2293	Energy Transfer System for Electric Vehicles
SAE J2836	Recommended Practice for Communication between Plug-in Vehicles and Utility Grid
SAE J1772	Electric Vehicle Conductive Charge Coupler
SAE J1773	Electric Vehicle Inductively Coupled Charging
IEC 62196	Plugs, socket outlets, vehicle couplers and vehicle inlets—Conductive charging of electric vehicles
IEEE 1547.3	Interconnecting Distributed Resources with Electric Power Systems

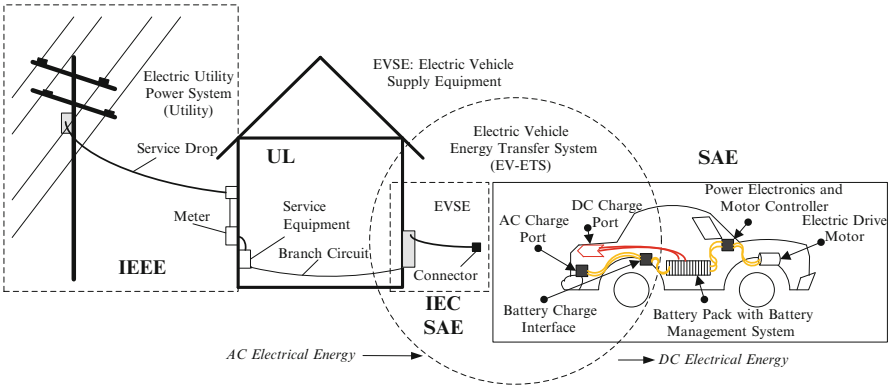

Fig. 2.3 Electric vehicle energy transfer system applicable standards. Modified from [9]

Table 2.4 EV charging power level

Charging level	Typical charging power
Level I	1.5–3 kW
Level II	10–20 kW
Level III	40 kW and up

In addition to the requirement of power quality (voltage, frequency, and harmonics) for EVs, the utility companies are most concerned about the charging power levels of EV. According to the Society of Automotive Engineers (SAE) Standard J1772, there are three charging levels, as shown in Table 2.4.

Level I and Level II are suitable for home. If, for example, one considers 2 kW as the average power demand of a typical home in North America, then the charging load of Level I is about 70–100% of the average home power consumption. The charging power of Level II can be over 5 times higher than that of Level II.

Table 2.5 EV charging schemes [10]

Features	V0G	V1G	V2G	V2B
Real-time communication		√	√	√
Communication with grid		√	√	
Timed charging		√	√	√
Backup source			√	√
Controllable load		√	√	√
Bidirectional grid ancillary service			√	
Load shifting for renewables			√	√

Therefore, it may be necessary to limit the charge rate to accommodate the rating of the on-board devices. For example, Chevy Volt and Nissan Leaf limit their charging rate to 3.3 kW [2].

Level III is for fast charging, which can give an EV 300 km range in one hour charging. The charger has to be off-board since the charging power can exceed 100 kW, which is significantly higher than Level I and Level II. It is obvious that Level III is not suitable for home use. However, it may be a better scheme for a company with a fleet of EVs. The total power and time that it takes to charge a group of EVs charged together at a low level can be the same as the fast charging of each vehicle in sequence. However, it is much more advantageous for an EV in the fleet can be charged quickly in less than 10 min.

Table 2.5 summarizes some of the various charging schemes of EV [10]. V0G is the most conventional one: plug in the vehicle and get it charged like any other regular load. V1G, also called smart charging, can charge the vehicle when grid allows or needs it to. There are communications between the grid and the vehicle. The smart grid concept with advanced metering infrastructure fits in this application well. Vehicles can communicate with advanced metering infrastructure (AMI) devices at home through home automation network (HAN); the AMI devices then communicate with the control center at the grid. V2G (vehicle to grid) is the most complicated scheme. In addition to the functions of V1G, it also allows the energy stored in the EV batteries to be delivered back to the grid for grid supports. V2B (vehicle to building) is similar to V2G. The difference is that in V2B, the vehicle does not communicate with the grid, but the building. The energy delivered back from the vehicle will be limited to the building.

2.5 Battery Chemistry

Various battery chemistries have been proposed as the energy source to power electrical vehicles since the 1990 California Zero Emission Vehicle was mandated, which required 2 and 10% of the automobiles sold to be zero emission in 1998 and 2003, respectively. These battery chemistries included improved lead–acid, nickel–cadmium, nickel–zinc, NiMH, zinc–bromine, zinc–chlorine, zinc–air, sodium–sulfur, sodium–metal chloride, and, later, Li-ion batteries, with each of

these chemistries having its own advantages and disadvantages. Towards the end of the last century, the competition between battery chemistries was resolved with General Motor's choice of NiMH for its EV-1 pure electrical vehicles. In the following decade, the technology of the HEV developed by Toyota and Honda matured and gained popularity through its combination of fuel economy, acceptable pricing, and clean safety record. Up to this date of 2011, the leading battery chemistry in these HEVs remains NiMH. As the concerns over greenhouse gas emissions and fossil energy shortages grow in the recent years, the development target has shifted from HEV to PHEV, with the eventual target being a purely battery-powered EV. The requirement of a higher energy density in PHEVs and EVs reopens the discussion for automobile battery technologies, giving Li-ion battery chemistry another chance at entering the electric car battery market. In this section, the underlying principles, the current market status, and the future developmental trends of NiMH and Li-ion batteries are discussed.

2.5.1 Basic Operation of a Rechargeable Battery

A battery is composed of a positive electrode (holding a higher potential) and a negative electrode (holding a lower potential) with an ion-conductive but electrically insulating electrolyte in between. During charging, the positive electrode is the anode with the reduction reaction, and the negative electrode is the cathode with the oxidation reaction. During discharge, the reaction is reversed, and so the positive and negative electrodes become cathode and anode electrodes, respectively. As a side-note, the positive and negative electrode active materials are also conventionally referred to as cathode and anode material, respectively. In a sealed cell, the liquid electrolyte is held in a separator to prevent the direct short between the two electrodes. The separator also serves as a reservoir for extra electrolyte, a space saver allowing for electrode expansion, an ammonia trap (in NiMH battery), and a safety device for preventing shortage due to Li-dendrite formation (in Li-ion battery).

A schematic of the NiMH rechargeable battery is shown in Fig. 2.4. The active material in the negative electrode is metal hydride (MH), a special type of intermetallic alloy that is capable of chemically absorbing and desorbing hydrogen. The most widely used MH in NiMH today is the AB_5 alloy with a $CaCu_5$ crystal structure, where A is a mixture of La, Ce, Pr, and Nd, and B is composed of Ni, Co, Mn, and Al. The active material in the positive electrode is $Ni(OH)_2$, which is the same chemical used in the Ni–Fe and Ni–Cd rechargeable batteries patented by Thomas Edison more than a hundred years ago. The intrinsic $Ni(OH)_2$ has a poor conductivity; to make up for this shortcoming, coprecipitation of other atoms, formation of conductive network outside the particle, or multilayer coating structure is implemented in the commercial product. The separator is typically made from grafted polyethylene (PE)/polypropylene (PP) non-woven fabric. The commonly used electrolyte is a 30 wt.% KOH aqueous solution with a pH value of about

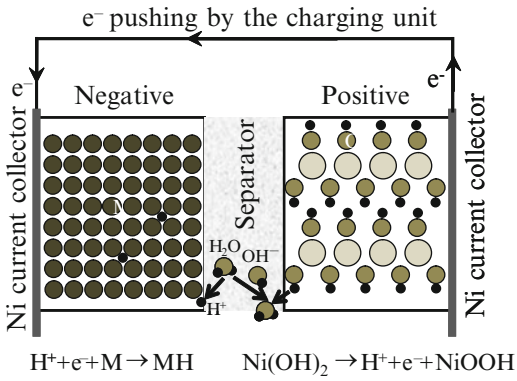

Fig. 2.4 Schematic of the charging operation of a NiMH battery

14.3. In some special designs for particular applications, certain amounts of NaOH and LiOH are also added into the electrolyte.

During charge, water is split into protons (H^+) and hydroxide ions (OH^-) by the voltage supplied from the charging unit. The proton enters the negative electrode, neutralizes with the electron supplied by the charging unit through the current collector, and hops between adjacent storage sites by the quantum mechanics tunneling. The voltage is equivalent to the applied hydrogen pressure in a gas phase reaction and will remain at a near-constant value before protons occupy all of the available sites. OH^- generated by charging will add to the OH^- already present in the KOH electrolyte. On the surface of the positive electrode, some OH^- will recombine with protons coming from the $Ni(OH)_2$ and form water molecules. The complete reaction for charging is as follows:

$$M + Ni(OH)_2 \rightarrow MH + NiOOH \tag{2.14}$$

Neither water nor OH^- is consumed; thus, no change to pH value occurs during charge/discharge. The oxidation state of Ni in $Ni(OH)_2$ is 2^+. As protons are consumed at the surface of the positive electrode, more protons are driven out of the bulk from both the voltage and the concentration gradients. Losing one proton increases the oxidation state of Ni to 3^+ in NiOOH. Electrons are collected by Ni-form or perforated Ni-plate and moved back to the charging unit to complete the circuit.

The whole process is reversed during discharge. In the negative electrode, protons are sent to the electrolyte and recombine with the OH^- as electrons are pushed to the outside load. The electrons reenter the positive electrode side of the battery through the outside load and neutralize the protons generated from the water split on the surface of the positive electrode.

A similar schematic with two half-cell reactions for the Li-ion battery in charging mode is shown in Fig. 2.5. The complete reaction is

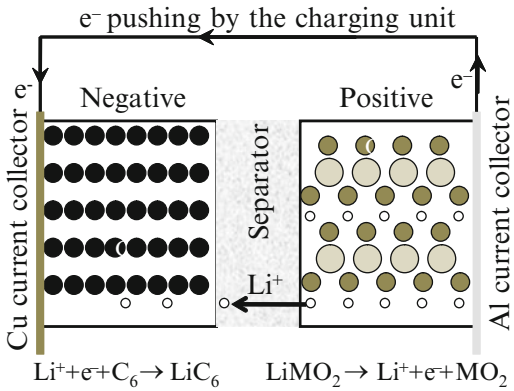

Fig. 2.5 Schematic of the charging operation of a Li-ion battery

$$C_6 + LiMO_2 \rightarrow LiC_6 + MO_2 \tag{2.15}$$

The most commonly used active material in the negative electrode is graphite. During charging, Li ions, driven by the potential difference supplied by the charging unit, intercalate into the interlayer region of graphite. The arrangement of Li^+ in graphite is coordinated by the surface–electrolyte–interface (SEI) layer, which is formed during the initial activation process. The active material in the positive electrode is a Li-containing metal oxide, which is similar to $Ni(OH)_2$ in the NiMH battery but replaces the hydrogen with lithium. During charging, the Li^+ (similar to the H^+ in NiMH) hops onto the surface, moves through the electrolyte, and finally arrives at the negative electrode. The oxidation state of the host metal will increase and return electrons to the outside circuitry. During discharge, the process is reversed. Li ions now move from the intercalation sites in the negative electrode to the electrolyte and then to the original site in the $LiMO_2$ crystal. The commonly used electrolyte is a mixture of organic carbonates such as ethylene carbonate, dimethyl carbonate, and diethyl carbonate containing hexafluorophosphate ($LiPF_6$). The separator is a multilayer structure from PP, which provides oxidation resistance, and PE, which provides a high-speed shutdown in the case of a short.

2.5.2 USABC Goals

USABC, composed of the Big Three (GM, Ford, and Chrysler) and a few National Laboratories belonging to the DOE, was established to develop the energy storage technologies for fuel cell, hybrid, and electrical vehicles. In the early 1990s, a set of performance targets was created and later modified. A few key qualitative goals set by the USABC for both the mid and long terms are listed in Table 2.6. One factor, specific energy, is important for the range a car can travel in one charge. The

Table 2.6 USABC battery performance goal

	USABC mid-term goal	USABC long-term goal	Impact on vehicle performance
Specific energy (Wh/kg)	150	200	Range and weight
Energy density (Wh/l)	230	300	Range and size
Specific discharge power (W/kg)	300	400	Acceleration and weight
Discharge power density (W/l)	460	600	Acceleration and size
Specific regenerative power (W/kg)	150	200	Energy saving and weight
Regenerative power (W/l)	230	300	Energy saving and size
Life (years)	10	10	Life-cycle cost
Life cycles	1,000	1,000	Life-cycle cost
Operation temperature (°C)	−40 to +50	−40 to 85	Life of battery
Selling price ($/kWh)	150	100	Acquisition and replacement costs

typical energy required for a car to drive a mile ranges from 0.25 kWh (GM's EV-1) to 0.30 (GM's Volt) and 0.33 kWh (Tesla's Roadstar). As an example calculation, a 200-l (50 gallons) battery pack with an energy density of 230 Wh/l can store 46 kWh of energy and travel 200 miles between charges. Another factor, power density, is important for acceleration and for the collection of regenerative energy from braking. The battery pack mentioned above, assuming a discharge power density of 460 W/l, can generate 92 kW (123 hp), which is acceptable for a typical passenger car.

With the exception of specific energy and selling price, all of the USABC mid-term goals were reached by the first-generation of Ovonic Battery Company's NiMH battery, which was installed on the EV-1. The specific energy of NiMH battery then was about 80 Wh/kg at the cell level, with the estimated cost at high volume production at $800/kWh. The near-term specific energy of 150 Wh/kg is still considered a formidable challenge for even today's top Li-ion battery used for propulsion purpose. The near-term cost target of $150/kWh remains unachievable but is becoming more attainable with improvements in today's technology.

The long-term goal of the USABC was set to replace conventional internal combustion engine cars with EVs; this attitude is reflected in the long-term goals set for battery specifications. For the same performance as the previously calculated example (46 kWh capacity battery and 123 hp electric motor), the weight of the battery can be reduced from 306 kg (when made with USABC's mid-term goal battery specifications) to 230 kg (when made with USABC's long-term goal battery specifications). Reductions in both the battery pack volume (200 to 152 l) and the selling price ($6,750 to $4,600) are also listed as long-term goals. These long-term goals are still challenging with today's technology.

Table 2.7 Comparison of HEV batteries from volume production

	NiMH	NiMH	Li-ion	Comment
Manufacturer	PEVE	PEVE	Hitachi	
Shape	Prismatic	Prismatic	Cylindrical	
Case material	Plastic	Metal	Metal	Metal case in NiMH improves 40% cooling performance
Cathode	$Ni(OH)_2$	$Ni(OH)_2$	$LiMn_2O_4$	
Anode	Rare earth AB_5	Rare earth AB_5	Amorphous carbon	
Cell capacity (Ah)	6.5	6.5	4.4	
Cell voltage (V)	1.2	1.2	3.3	Plastic-cased NiMH is a 6-cell module and the metal-cased NiMH is a 8-cell model
Specific energy (Wh/kg)	46	41	56	
Specific output power (W/kg)	1,300	1,200	3,000	
Operation temperature (°C)	−20 to +50	−20 to +50	−30 to +50	
Market	Toyota-HEV	Toyota-HEV	GM-HEV (2012)	

2.5.3 Performance Comparison Between NiMH and Li-Ion Batteries in PHEV

While many exciting results are being presented on the performance of emerging battery technologies, the majority of them come from laboratory reports based on small-scale test runs. In order to fairly compare the performances of NiMH and Li-on, the batteries currently in mass production by two reputable manufacturers were selected. Key performance statistics from the NiMH battery by Primearth EV Energy Co. [11] and the Li-ion battery by Hitachi Vehicle Energy Ltd. [12] are listed in Table 2.7. Two types of NiMH batteries, plastic and metal-cased, are shown here. The latter was introduced to trade 10% of the energy and power densities for a 40% improvement in cooling efficiency. A quick glance through the data reveals that the advantages of Li-ion are obvious: higher specific energy and output power.

However, with a closer look at the comparison of specific energies, the superiority of Li-ion is limited at the current development stage. At the cell level, the specific energy of Li-ion is about 20% higher than that of NiMH. However, after taking the two batteries' cooling mechanisms into consideration, the air-cooled NiMH may have a higher specific energy at the system level since, in order to optimize its service life, the Li-ion battery requires a powerful liquid-cooling structure that adds the weights of the coolant, compressor, evaporator, and controller to the system weight. Moreover, the battery management system for NiMH is on the system level, making it simpler and lighter than Li-ion's management system, which demands precise control at the cell level. An additional concern is that Li-ion

needs to be overdesigned to overcome its short calendar life issue (as seen in the GM Volt where only 50–70% of its energy is "usable" to ensure it has an acceptable calendar life), while NiMH does not. From the more practical perspective of looking on the car level, the current Li-ion (battery pack) does not necessarily provide a higher specific energy. This observation explains the difference in driving range between the recently developed Li-ion battery powered Nissan Leaf EV (80–100 miles) and the fifteen-year-old NiMH battery powered EV-1 (180 miles).

Another point that needs to be addressed is the comparison in power performance. The data shown in the table compare the two batteries' output power, which assists the engine in PHEV during acceleration. As for input power, both NiMH and Li-ion batteries have the same impedance during charge and discharge, as opposed to the lead–acid battery, which has a charging impedance three times higher than its discharge impedance. Theoretically, a Li-ion battery should be able to take in 3,000 W/kg power during braking. However, in the modern Li-ion battery management systems, a safety factor of 3 is normally applied in order to reduce the risk of Li-dendrite formation and excessive heating of the battery. Therefore, in real cases, the maximum input power for Li-ion is limited to 1,000 W/kg at the cell level, with that number being further decreased after considering the added weight from the cooling system and controller.

From the published data, there seems to be little difference between NiMH and Li-ion batteries in power and energy performance. However, other factors such as calendar life, cycle life under realistic conditions, and, most importantly, abuse tolerance in aged battery packs (which may show the dangerousness of a degraded SEI layer in the Li-ion battery) are not available. Fair comparisons of these additional factors may be made only after the Li-ion battery technology has been used for many years, which may not be until the year 2022 when the GM PHEV celebrates its ten-year anniversary.

2.5.4 Current Status of Battery in Automobile Applications

NiMH batteries, mainly made by Sanyo and Primearth EV Energy Co. (PEVE), dominate the mass production lines of today's HEVs. While batteries from PEVE are prismatic (rectangular shaped), those made by Sanyo are cylindrical (standard D-size). Other NiMH manufacturers are entering the HEV market now, including Gold Peak, Corun, and TMK; however, both endurance and product consistency have yet to be proven for the batteries of these newcomers.

In PHEVs, a relatively new application for batteries, both Gold Peak (NiMH) and A123 ($LiFePO_4$) supply batteries for third parties to produce range extenders for the Prius. GM introduced the first commercial purpose-built PHEV built at the end of 2010 with batteries from LG Chemical ($LiMn_2O_4$). More prototype PHEVs made by various car manufacturers and OEMs use either Li-ion or NiMH to provide part of the power source.

Table 2.8 Li-ion battery cathode and anode material comparison

Material	Specific capacity, mAh/g	Voltage vs. L^+/Li, V	Characteristics
$LiCoO_2$	160	3.7	Most commonly used in consumer product, good capacity and cycle life, but expensive and unsafe upon fast-charge
$LiMn_2O_4$	130	4.0	Most commonly used in automobile, low cost, acceptable rate capability, poor cycle and calendar life
$LiFePO_4$	140	3.3	Low cost, improved abuse tolerance, good cycle life and power capability, but low capacity and calendar life
NMC	180	4.2	Lowest cost, high capacity, life is less than NCA
NCA	185	4.2	Highest capacity, low cost, but safety concerns
Graphite	372	0.0–0.1	Most commonly used in all applications, low cost
LTO	168	1.0–2.0	Highest cycle and calendar life, but costly and low in energy density
Silicon	3,700	0.5–1.0	Still in research stage, high energy, but large volume expansion during charging needed to be solved

Besides the obsolete EV-1, there are currently two pure EVs available on the market. One is the luxury Roadster (retailing for $109,000 in the USA) introduced by Tesla Motors; it is equipped with 6,831 small cylindrical Li-ion ($LiMn_2O_4$) batteries (size 18650) in 2008. The other is the Nissan Leaf (retailing for $32,780 in the USA), which has 192 prismatic Li-ion ($LiMn_2O_4$) cells from AESC.

While the chemistry of NiMH batteries was finalized fifteen years ago, this is not so for the Li-ion batteries for propulsion applications: the debate over which cathode or anode materials are better is still continuing. The issue is that none of the candidates are perfect; moreover, there are patent issues for a few key chemistries. Table 2.8 lists a few major candidates for cathode and anode materials.

Among the cathode materials, $LiCoO_2$ is the most popular one used in today's notebook computer, but it is notorious for catching on fire. $LiMn_2O_4$, widely used in cell phones, is low in specific energy and poor in both cycle life and calendar life. $LiFePO_4$, with improvements in both abuse tolerance and power capability, also suffers from low energy (both capacity and voltage) and short calendar life. Both Li (Ni, Mn, Co)O_2 (NMC) and Li(Ni, Co, Al)O_2 (NCA) are new additions to the list, but still have concerns in calendar life and abuse tolerance.

Among the anode materials, graphite is the most common. Although graphite has a relatively high specific energy and a low cost, it has an unstable SEI layer [13], especially at higher SOCs and elevated temperatures (>40°C), which causes severe performance degradation, especially in the output power. $Li_4Ti_5O_{12}$ (LTO) or the similar Li–Ti oxides provide solutions to both the cycle life and calendar life issues of graphite; however, the specific capacity of LTO is only half of that of graphite, and its half-cell potential is at least 1.0 V higher than graphite.

The specific energy is determined by both the specific capacity in Ah and the voltage of the cell. The voltage of a cell is the difference in potentials between

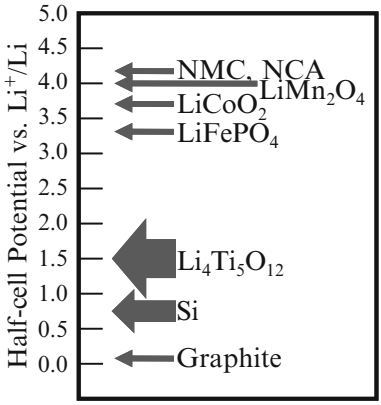

Fig. 2.6 Half-cell potentials of active material in Li-ion battery

cathode and anodes. The potentials of the materials listed in Table 2.8 are plotted in Fig. 2.6 to address the issue of cell voltage. The combination optimized for the greatest abuse tolerance ($LiFePO_4$ + LTO) gives a cell voltage of 1.9 V, which is less than half of 4.0 V, the voltage obtained from other combinations. Safer Li-ion batteries come at the cost of having significantly lower specific energy than unsafe ones do. Today, the balance between performance and safety remains a major challenge to the implementation of Li-ion technology in the propulsion application.

2.5.5 Development Trend of Battery Used in EV

The Regone plot (specific energy vs. specific power) shown in Fig. 2.7 summarizes the current status and the future outlook of batteries in propulsion application. While the advantages of Li-ion over NiMH and lead–acid in both specific energy and power are obvious, the potential of super-capacitors in very high power applications cannot be overlooked. One developmental effort will be to combine the superior specific energy offered by the battery with the superior specific power offered by the super-capacitor. The super-capacitor so offers a cache energy for fast access and shields the battery from very fast fluctuation [14].

The USABC requirements for HEV, PHEV, and BEV [15] are described in Fig. 2.7. While both the HEV and PHEV goals are either already reached or are close to being accomplished by both Li-ion and NiMH batteries, the goals for BEV are far beyond today's technology. The following paragraph is a review of the developmental trend of BEV battery in three different systems: NiMH, Li-ion, and metal–air batteries.

The current research on NiMH for EV application is focused on the following areas: MH alloy, γ-phase NiOOH, nonaqueous electrolyte, and bipolar structure. While the first two areas aim at reaching higher specific energies, the other two

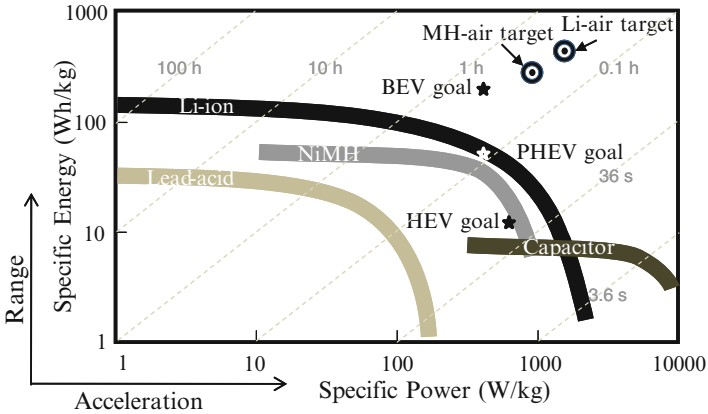

Fig. 2.7 Regone plot of a few electrochemical energy storage devices used in the propulsion application

target higher power densities. The currently used AB_5 MH alloy has a hydrogen storage capability of 1.2 wt.%, which is equivalent to an electrochemical storage of 322 mAh/g. The potential replacements for AB_5 are A_2B_7 (1.5 wt.%), AB_2 (2.0 wt.%), Ti–V–Cr solid solution (3.0 wt.%) and MgNi-based alloy (3.6 wt.%). A half-cell capacity of over 790 mAh/g was demonstrated from the combination of melt-spin and mechanical alloying for MgNi [15]. In the positive active material, the current β-$Ni(OH)_2$-NiOOH transition can supply one hydrogen per Ni, while γ-NiOOH can supply up to 1.7 hydrogen per Ni. The conventional γ-NiOOH is obtained by inserting water molecules together with some anions between the NiO_2 planes, which causes a large lattice expansion and deteriorates the cycle life. New γ-phase can be formed without expanding the lattice by doping the host $Ni(OH)_2$ matrix with other elements [16]. In the electrolyte, the operation voltage of current NiMH batteries is limited by the electrolysis of H_2O. Replacing water-based electrolyte with proton-conducting liquid gel or solid membrane enables the use of positive and negative active materials with much higher voltages. Recent reports on some oxide films capable of storing hydrogen are promising [17–19]. The last research area for NiMH is the bipolar structure. Although the theoretical charge/discharge rate of NiMH is very high, it is limited by the heat transfer in the cell. By adopting a bipolar structure with cooling water running through the connection plate, Kawasaki is able to increase the power capability of NiMH substantially [20]. G4 Synergetic is also working on a special design of bipolar NiMH battery [21].

Current research endeavors in Li-ion battery for EV application are similar to those of NiMH: new high capacity metal oxide cathode, high capacity anode, and new electrolyte with high oxidation potential. In the cathode material, only about 50% of the Li is currently pulled out during each charge operation. With high charging voltage, more Li can be transferred to the anode, and the capacity can be increased. In the anode area, Si has a very high theoretical capacity (about ten times

that of graphite); however, the lattice expansion after a full charge can be as high as 270%. Alloying Si with an inert ingredient or depositing Si onto some types of supporting structures may be feasible solutions for realizing the ultrahigh capacity of Si. The third area of interest is the electrolyte: similar to the case of NiMH, the cell voltage of Li-ion battery is limited to 4.2 V at which the solvent starts to be oxidized. The adoption of a new electrolyte with a higher oxidation potential will enable the use of high-voltage cathodes, such as $LiCoPO_4$ [22] and $LiNi_{0.5}Mn_{1.5}O_4$ [23], which can increase the specific energy.

The last approach is about the metal–air batteries. Replacing the positive electrode with an air electrode from the fuel cell can substantially reduce the weight of the battery and increase both specific power and energy. This is a feasible approach to achieve the USABC EV goal. Both the potential goals of Li–air and MH–air batteries are indicated in Fig. 2.7. In this arena, Ovonic Battery Company has shown a prototype of MH–air battery capable of delivering 200 Wh/kg [24], and MIT has demonstrated a Li–air battery with a specific energy as high as 2,500 Wh/kg [25].

2.6 Battery Modeling

Battery modeling forms the basis of and stands as an effective tool for battery design, manufacturing, and control. It is particularly important for battery characterization (such as SOC and SOH estimation) and battery management since the model development is logically the first step in developing any system identification and state estimation algorithms.

Extensive research has been carried out on battery modeling and a variety of models have been developed from different aspects and for different purposes [26–47, 55]. The most common models can be generally classified into two groups: electrochemical models and equivalent circuit models. Detailed electrochemical models are normally targeted for the fundamental, physical aspects of batteries and most of them are static models. Some of these models are developed using finite element analysis to investigate the complexity of the electrochemical processes inside a battery. They are suitable for battery design, but not appropriate for dynamic simulation studies over a long time. On the other hand, electric circuit models are normally lumped-parameter models and developed for long-time simulation studies. Electrical engineers favor electric circuit models since the models are more intuitive and can be incorporated with other circuit devices for circuit design and simulation studies.

For the studies of EV system integration, control, optimization, and the interconnection of EVs to grid, lumped-parameter models are well-received. In those studies, the battery terminal and overall characteristics and dynamics including voltage, current, temperature, and SOC are more of interest than the detailed electrochemical reactions inside the battery. In this subsection, the focus is given to lumped-parameter circuit models of battery. Equivalent circuit models,

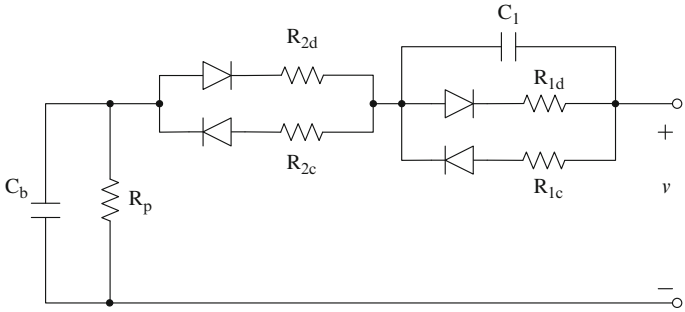

C_b = battery capacitance, R_p = self-discharge resistance, or insulation resistance, R_{2c} = internal resistance for charge, R_{2d} = internal resistance for discharge, R_{1c} = overvoltage resistance for charge, R_{1d} = overvoltage resistance for discharge, C_1 = overvoltage capacitance.

Fig. 2.8 Equivalent circuit model of battery reported in [36]. C_b = battery capacitance, R_p = self-discharge resistance, or insulation resistance, R_{2c} = internal resistance for charge, R_{2d} = internal resistance for discharge, R_{1c} = overvoltage resistance for charge, R_{1d} = overvoltage resistance for discharge, C_1 = overvoltage capacitance

consisting of electrical circuit components such as capacitors, resistors, diodes, and voltage sources, can be readily developed using electric circuit simulation software such as PSpice. Other types of models, given in algebraic or differential equations, may be more suitable for a generic simulation environment such as Matlab/Simulink. Matlab also released a generic battery model in its SimPowersystems toolbox [46, 68]. Nevertheless, an equivalent circuit model can be easily converted into other model formats. The choice of model representation will be determined by the matter of convenience and the simulation tools available.

2.6.1 Equivalent Circuit Models of Battery

Ideally, a battery can be represented as an ideal voltage source, which we have seen in various "electric circuit" textbooks. A more practical way but still ideal is to model battery using a resistive Thevenin equivalent circuit: a voltage in series with a resistor. These two are the simplest types of models and have been widely used in electric circuit analysis and design. However, they are oversimplified and cannot give any detailed and accurate information about the battery operation and performance such as the battery SOC, thermodynamics, etc. More advanced circuit models have been proposed for batteries.

A validated electrical circuit battery model, shown in Fig. 2.8, was reported in [36]. The diodes in the model are all ideal and just used to select different resistances for charging and discharging states. The values of model parameters (capacitances and resistances) defined in Fig. 2.8 are functions of actual electrochemical reactions

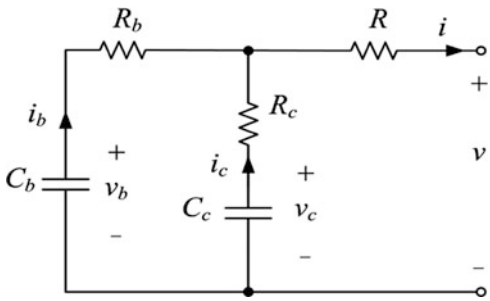

Fig. 2.9 NREL battery model [47]

and temperature dependent [36]. A least square algorithm and a temperature compensation formula were used to accommodate the variations [36].

$$BE = k_1 \exp\left[k_2(V_m - V_{oc})\right]^{k_3}, \tag{2.16}$$

where BE represents the battery elements modeled in Fig. 2.8; V_{m} is the mean voltage level; V_{oc} is the open circuit voltage; and k_1, k_2, and k_3 are the factors determined by the least square algorithm. For instance, the battery capacitance can be represented as $C_b = k_{1,cb} \exp[k_{2,cb}(V_m - 14.0)^{k_{3,cb}}]$ when the V_{oc} is 14 V. Quantities $k_{1,cb}$, $k_{2,cb}$, and $k_{3,cb}$ are the empirical factors determined by the actual data via the least square curve fitting [36].

The temperature effect on resistors was compensated using

$$TC = \left(\frac{R}{R_{ref}}\right)^{\frac{T_{ref}-T}{T_{ref}}}, \tag{2.17}$$

where TC is the temperature compensation factor, R is the resistance at temperature T, and R_{ref} is the resistance value at the reference temperature T_{ref}.

The model given in Fig. 2.8 was developed for lead acid batteries, but it can be extended to model other types of battery. However, the model does not provide a way to estimate the SOC of battery. Though the parameters can be adjusted for different operating conditions, the correction given in (2.14) and (2.15) may not be accurate, which may limit the applications of the model.

National Renewable Energy Laboratory (NREL) also developed an electric circuit model for batteries, as a part of its ADVISOR tool package [47]. The model, shown in Fig. 2.9, is basically a RC network. The model contains two capacitors (C_b and C_c) and three resistors (R_b, R_c, and R). The capacitor C_b models the main storage capacity of the battery. The capacitor C_c captures the fast charge–discharge aspect of the battery and is much smaller than C_b.

The electric circuit model can be converted into other model formats for the convenience of simulation. For example, the circuit model in Fig. 2.9 can be expressed using a state space model. The electric circuit and thermodynamic variables in the circuit model are defined in Table 2.9.

Table 2.9 Variables used in the NREL circuit model of battery

Symbols	Description
v	Terminal voltage (V)
i	Terminal current (A)
v_b	Voltage of the capacitor C_b (V)
i_b	Current through the capacitor C_b (A)
v_c	Voltage of the capacitor C_c (V)
i_c	Current through the capacitor C_c (A)
T_a	Air temperature (°C)
T	Cell temperature (°C)
q_c	Conducting heat transfer rate (W)
q_b	Heat transfer rate generated by the battery cell (W)
q_{ac}	Air conditioning forced heat transfer rate (W)
R_T	Equivalent thermal resistance (°C/W)
C_T	Equivalent heat capacitance (J/°C)
S	SOC
S_b	SOC_{Cb}
S_c	SOC_{Cc}
η	=1, charge =0, discharge

The following basic circuit equations can be obtained for the circuit:

$$\begin{cases} C_b\dot{v}_b = -i_b \\ C_c\dot{v}_c = -i_c \\ v_b - i_bR_b = v_c - i_cR_c \\ i = i_b + i_c \\ v = v_c - i_cR_c - iR \end{cases}. \tag{2.18}$$

The battery thermal model is represented by a lumped first-order equation with linear dynamics:

$$\begin{cases} q_c = \dfrac{T - T_a}{R_T} \\ C_T\dot{T} = q_b - q_c - q_{ac} \end{cases}. \tag{2.19}$$

The parameters of the components are functions of the SOC and battery temperature (T). In addition, the resistance also depends on whether the battery is in "charge" or "discharge" mode. The overall SOC is a weighted combination of the states of charge on C_b and C_c:

$$S = \alpha_b S_b + \alpha_c S_c, \tag{2.20}$$

where $\alpha_b + \alpha_c = 1$. In the NREL model, $\alpha_b = 20/21$ and $\alpha_c = 1/21$ [47]. S_b and S_c are functions of v_b and v_c, i.e., $S_b = g_b(v_b)$ and $S_c = g_c(v_c)$, respectively. The circuit parameters can be expressed in general as

$$\begin{aligned} &R_b = f_{Rb}(v_b, v_c, T, \eta),\ R_c = f_{Rc}(v_b, v_c, T, \eta),\ R = f_R(v_b, v_c, T, \eta), \\ &C_b = f_{Cb}(v_b, v_c, T),\ C_c = f_{Cc}(v_b, v_c, T) \end{aligned}. \tag{2.21}$$

These condition-dependent parameters can be experimentally established or identified through system identification methods as discussed later in this chapter.

Choose v_b, v_c, and T as the state variables; inputs are i (battery current), T_a (air temperature), q_b (battery cell generated heat flow rate), and q_{ac} (convective heat flow rate due to cooling air); and outputs are v (terminal voltage), S (the overall SOC), and the battery temperature (T). The state space representation of the model can be obtained as

$$\begin{cases} \dot{v}_b = \dfrac{v_b - v_c}{(R_b + R_c)C_b} + \dfrac{R_c}{(R_b + R_c)C_b} i \\ \quad = f_1(v_b, v_c, T, \eta) + g_1(v_b, v_c, T, \eta) \\ \dot{v}_c = \dfrac{v_c - v_b}{(R_b + R_c)C_c} + \dfrac{R_b}{(R_b + R_c)C_c} i \\ \quad = f_2(v_b, v_c, T, \eta) + g_2(v_b, v_c, T, \eta) \\ \dot{T} = \dfrac{1}{C_T} q_b - \dfrac{1}{C_T R_T} T + \dfrac{1}{C_T R_T} T_a - \dfrac{1}{C_T} q_{ac} \\ v = \dfrac{R_b v_c + R_c v_b}{R_b + R_c} - \left(\dfrac{R_b R_c}{R_b + R_c} + R \right) i \\ \quad = h_1(v_b, v_c, T, \eta) + m_1(v_b, v_c, T, \eta) \\ S = \alpha_b S_b + \alpha_c S_c \\ T = [0\,0\,1][v_b\, v_c\, T]' \end{cases}. \tag{2.22}$$

Denote the state vector by $x = [v_b, v_c, T]'$, input vector $u = [i, T_a, q_b, q_{ac}]'$, and output vector $y = [v, S, T]'$. The state space model can be rewritten in general as

$$\begin{cases} \dot{x} = f(x, \eta) + g(x, \eta)u \\ y = h(x, \eta) + m(x, \eta)u \end{cases}. \tag{2.23}$$

The system given in (2.23) is a nonlinear system in an affine form. It is also a hybrid system since η is a discrete value for "charge" or "discharge" mode operation of a battery.

2.6.2 Future Development Needs of Circuit Model for Batteries

It would be desirable to have a comprehensive, unified electrical model that is developed based on physical properties of battery cells. The model should have the capability to estimate SOC and SOH accurately. A conceptual, unified model with

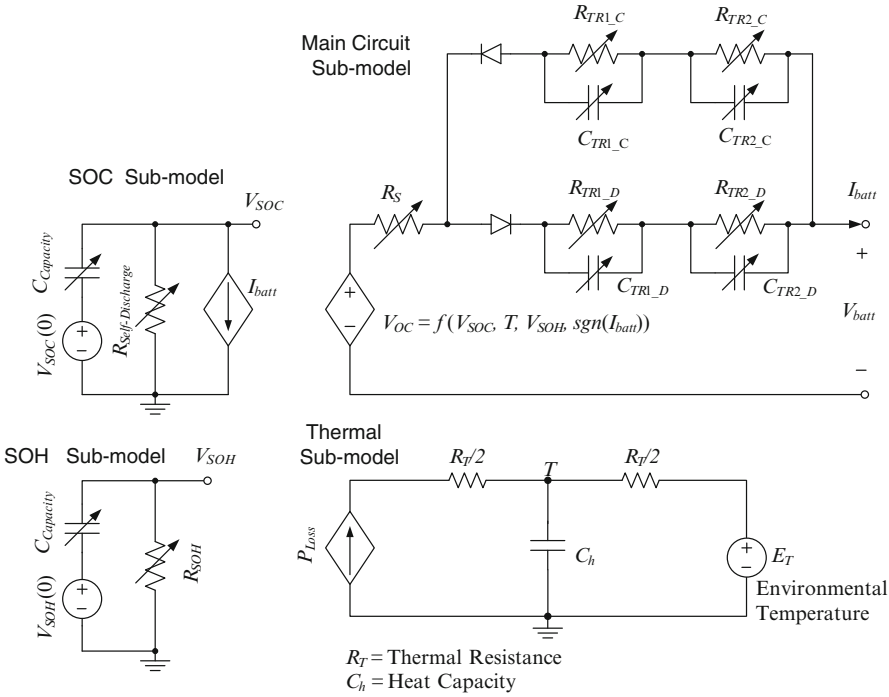

Fig. 2.10 A conceptual unified electrical circuit model of battery

the above desired features, shown in Fig. 2.10, consists of four parts: Main circuit, thermodynamic, SOC, and SOH sub-models.

In the main circuit sub-model, the charging and discharging processes will have different transient paths selected by the two diodes. The two RC circuits in either path are used to model the dynamic responses to load transients. For example, in the discharging path (denoted with subscript "*D*" in the figure), $R_{\mathrm{TR_1_D}}$ and $C_{\mathrm{TR_1_D}}$ are for a slow transient response, while $R_{\mathrm{TR_2_D}}$ and $C_{\mathrm{TR_2_D}}$ are for a faster one. The open circuit voltage V_{OC} is a function of SOC, SOH, and the battery temperature. V_{OC} will be obtained based on physical electrochemical properties of batteries. The circuit component values (R values and C values) are all functions of SOC, SOH, and temperature in general. The circuit values can be estimated through the state estimation method discussed later in the chapter.

The SOC and SOH sub-models will be used to indicate the SOC of a battery and to predict its SOH. $V_{\mathrm{SOC}} = 1$ V corresponds to 100% of SOC and 0 V to 0%. The SOC will decrease as the battery is being discharged or self-discharges. The capacity capacitance (C_{Capacity}) is one of the most important parameters in the circuit model and its value is a function of SOC, SOH, and battery temperature. C_{Capacity} and other important parameters including the initial values of V_{SOC} and V_{SOH}, self-discharging resistance ($R_{\mathrm{Self\text{-}Discharging}}$), and lifetime deterioration equivalent resistance R_{SOH} will also be experimentally determined or estimated by the state estimation method and can be loaded externally before the simulation.

The analogies between the thermodynamic and electrical quantities [48] are employed to develop the thermodynamic sub-model. The input current source represents the battery loss, which can be simply estimated as $P_{Loss} = |V_{OC} - V_{batt}| \times I_{batt}$. The thermal resistance (R_T) due to air convection is split into half in the circuit and C_h is the lumped heat capacity of the battery. In Fig. 2.10, the constant voltage source E_T represents the environmental temperature, and the voltage across the capacitance (C_h) is the overall temperature of the battery.

It is a very challenging task to develop a model that is capable of predicting SOH and gauging SOC. At the same time, for investigating EVs as part of the grid, modularity of the model is also very important. A battery model needs either to be modular or upgradable so that a large battery system model can be readily developed based on the module model without fundamental changes. Future research efforts are required to address these needs in battery modeling.

2.7 Run-Time Battery Characterization and Management

Battery management systems (BMS) make decisions on charge/discharge rates on the basis of load demands, cell voltage, current, and temperature measurements, and estimated battery SOC, capacity, impedance, etc. Within these variables, the SOC is the most critical indicator. This is especially important for Li-ion batteries since their overcharge can accelerate battery degradation, catch fire, or, in a worst-case scenario, even cause explosion. On the other hand, over-discharge can result in loss of capacity and shortening of cell life. In EV applications, frequent charge/discharge cycles are common. To maintain the capability of absorbing returning energy from regenerative braking and large torque delivery in fast vehicle acceleration or cold-start, the SOC must be sustained in a middle range such as 40–75%.

2.7.1 SOC Estimation [69]

At present, most BMS rely on cell voltage regulation as a means of controlling SOC. This becomes more difficult for Li-ion batteries since their cell voltages vary only slightly in the middle range (before the "knee section" of the voltage-capacity curve). Consequently, many modified methods have been introduced and explored to improve SOC estimation. Typical methods include inverse mapping using the SOC-to-voltage characterization curves, computation of amp-hours by using load current integration, impedance measurements, and more advanced extended Kalman filtering (EKF) [49–53].

Here, an adaptive SOC observer that uses gain-scheduled pole placement design is described [69]. A special case of the general model representation given in (2.23) is a battery model that can be described by a state space model with a linear state equation and a nonlinear output equation, given below in (2.24).

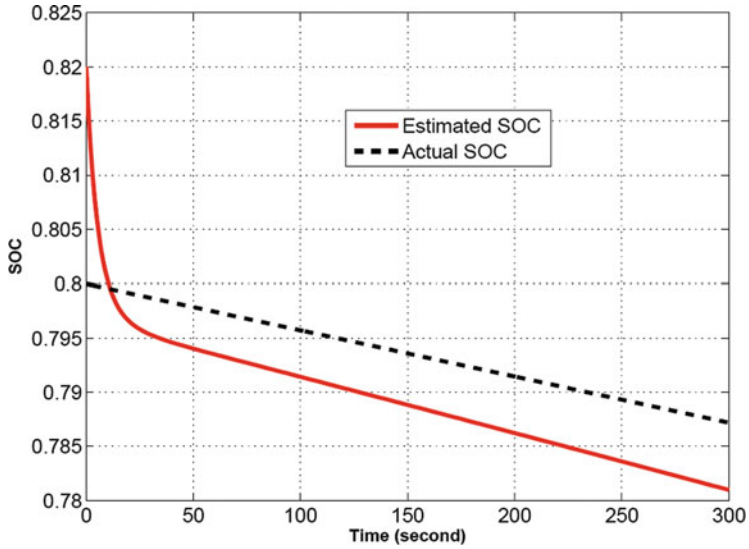

Fig. 2.11 Nonadaptive observer design under a constant discharge current [69]

An example model of (2.24) is the battery model in the SimPowerSystems Toolbox in Matlab/Simulink [47, 68].

$$\begin{aligned} \dot{x} &= Ax + Bi(t), \\ v &= f(x, i), \end{aligned} \tag{2.24}$$

where the input is the current load i, the output is the cell voltage v, and the state variable x contains SOC as one of its component. As a result, SOC estimation is now a state observation problem. The adaptive state observer has the structure

$$\begin{aligned} \dot{\tilde{x}} &= A\tilde{x} + Bi(t) - L(\tilde{x})(\tilde{v} - v), \\ \tilde{v} &= f(\tilde{x}, i). \end{aligned} \tag{2.25}$$

Here, the observer feedback gain matrix L is adjusted according to the estimated state. This is called a gain-scheduled feedback which is a special scheme of adaptation. Consequently, this observer is adaptive. The gain matrix L is designed, for each estimated state, such that the state estimation error $e = \tilde{x} - x$ has a stable dynamics, namely, it approaches zero asymptotically. One possible design is to place the poles of the closed-loop system for the error dynamics at selected stable locations (in the left half of the complex plane). This is called pole placement design [54]. Together, this becomes a gain-scheduled SOC estimator.

To illustrate its utility, the demonstration Li-ion model in the SimPowerSystems Toolbox in Matlab/Simulink for such battery models [47, 68] is used. Figure 2.11 provides the evidence why nonadaptive observers with a constant matrix L are not adequate for SOC estimation. Figure 2.12 demonstrates

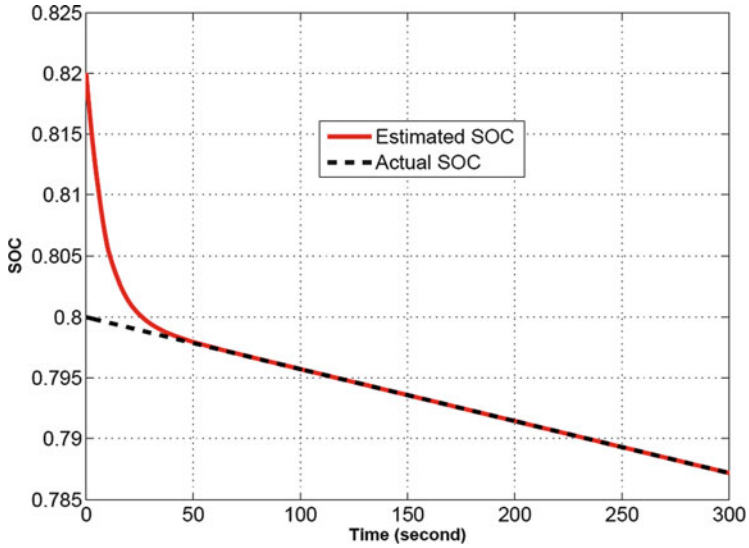

Fig. 2.12 Adaptive SOC observer design under a constant discharge current [69]

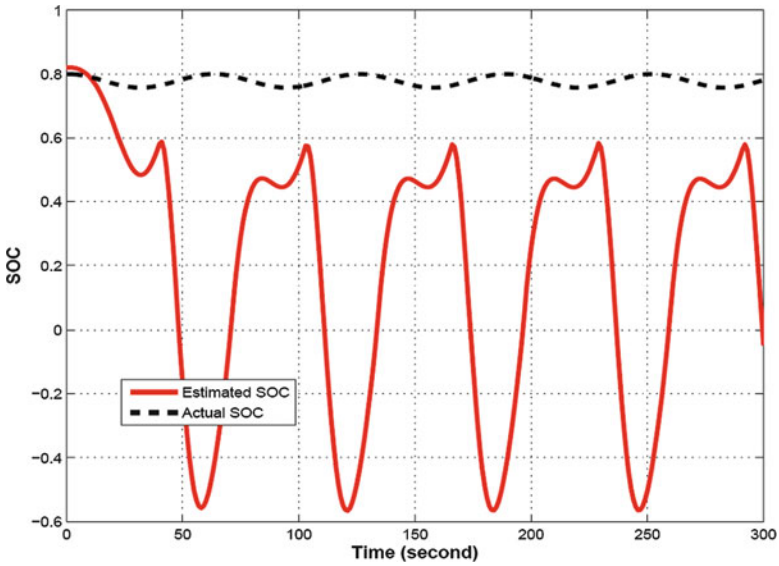

Fig. 2.13 Nonadaptive observer design under a cyclic charge/discharge current [69]

the accuracy of an adaptive SOC estimator. Similar comparison can be made between nonadaptive observer design in Fig. 2.13 and adaptive design in Fig. 2.14 for tracking the SOC in a cyclic charge–discharge operation. Further details of this methodology can be found in [54].

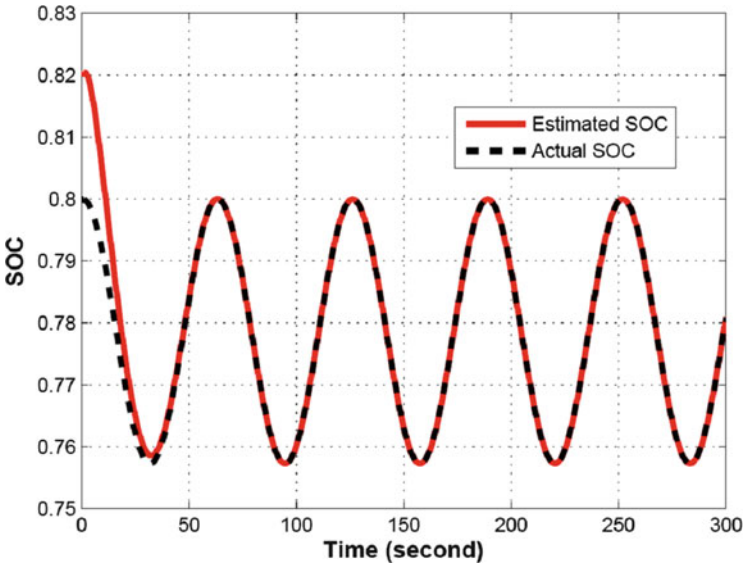

Fig. 2.14 Adaptive observer design under a cyclic charge/discharge current [69]

2.7.2 Run-Time and Cell-Level Individualized Battery Characterization

An EV battery system consists of many battery cells, which always have different characteristics. When manufacturers package battery cells into packs, efforts are often made to group cells of similar capacity and characteristics (often from the same batch) so that cell-to-cell variations are minimized for new battery packs. However, battery cells change with time and operating conditions due to a variety of factors such as aging, operational conditions, and chemical property variations. Consequently, during operating cycles over an extended time, SOC, battery health, remaining life, charge and discharge resistance, and capacitance demonstrate nonlinear and time-varying dynamics [49, 51, 55–57]. Consequently, for enhanced battery management, reliable system diagnosis, and improved power efficiency, it is desirable to capture individualized characteristics of each battery cell and produce updated models in real time. This is a problem of system identification [58, 59].

To facilitate model updating during run time, we first represent a linearized battery model in its input/output form, namely, a transfer function [60]. Since most battery models are either first-order or second-order and involve an integration of the input current, the typical form is

$$\frac{V(s)}{I(s)} = \frac{d_1 s^2 + d_2 s + 1}{c_1 s^2 + c_2 s}. \tag{2.26}$$

This can be conveniently modified to

$$H(s) = \frac{I(s)/s}{V(s)} = \frac{c_1 s + c_2}{d_1 s^2 + d_2 s + 1}. \tag{2.27}$$

This step relates the total charge or discharge to the voltage and makes the transfer function strictly proper, which is more suitable for system identification. $H(s)$ is then discretized for a given sampling interval, which is usually the actual sampling interval of the data acquisition system for the battery system, although other choices can be accommodated. This leads to a discrete-time system of transformed input–output variables u and y:

$$\frac{Y(z)}{U(z)} = \frac{b_1 z + b_2}{z^2 + a_1 z + a_2}, \tag{2.28}$$

which can be equivalently written in a regression form:

$$y_k = -a_1 y_{k-1} - a_2 y_{k-2} + b_1 u_{k-1} + b_2 u_{k-2} = \phi_k^T \theta. \tag{2.29}$$

Here, $\phi_k^T = [-y_{k-1}, -y_{k-2}, u_{k-1}, u_{k-2}]$ is called the regressor which is updated by the measurement data at each sampling time and $\theta^T = [a_1, a_2, b_1, b_2]$ is the model parameter vector that is to be updated. This regression form allows us to apply many standard identification algorithms and analyze their accuracy, convergence, and convergence speed, which are essential properties to ensure that updated models are authentic and accurate. For example, one may choose to use the Recursive Least Squares (RLS) estimation algorithm, as reported in [58].

To illustrate, the RLS estimation was applied to update the model parameters for the battery system in [47]. The model parameters are identified and the model output is compared to the true system. Convergence of parameter estimates are shown in Fig. 2.15.

2.7.3 Cell Balancing

Cell balancing is an essential function of BMS, especially for Li-ion batteries [61–64]. To supply required voltages, battery cells must be connected in series. During charge and discharge, each cell in the string will be subject to the same current, but will have different SOCs due to several factors. First, cells have different capacities. Even if the manufacturer makes the best effort to match capacities for new cells, nonuniform operating conditions impose different thermal and electrical stress on cells, causing changes in capacities. Although Li-ion cells have small self-discharge, small differences can accumulate over time, causing

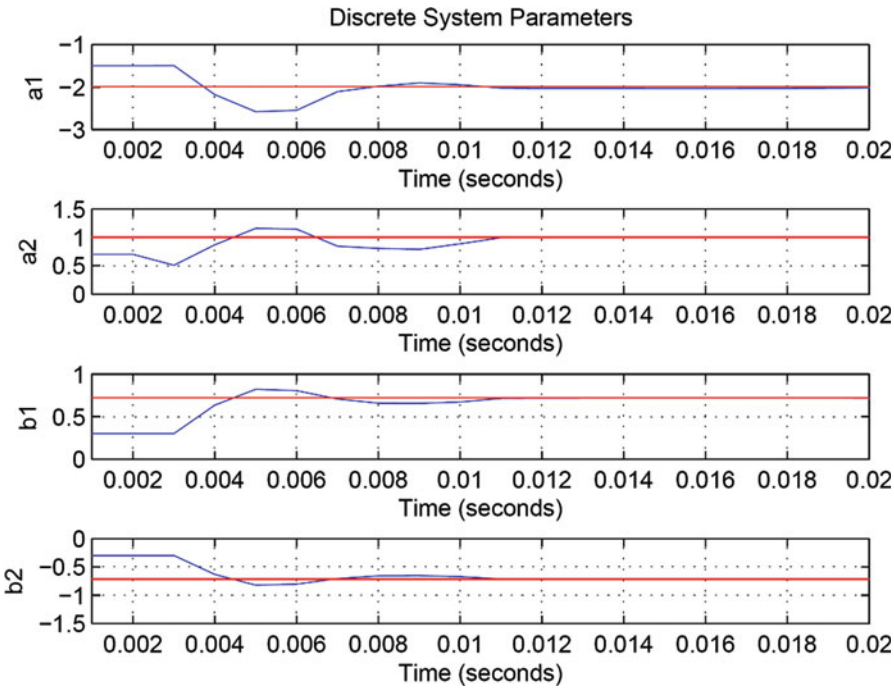

Fig. 2.15 Comparison of the model parameter estimates and the true model parameters (a simulated battery system with parameters established from lab experiments by NREL)

different SOCs even for cells with nearly identical capacities. Furthermore, variations in internal impedance and material aging inevitably lead to nonuniform cell characteristics. To protect the cells from overheat, overcharge, and overdischarge, the operation of the string is fundamentally limited by the weakest cell, the one reaches SOC upper and lower boundaries first. Such an imbalance prevents cells to supply their capacities fully, and consequently limits the battery run time, SOH, and life cycles.

Cell balancing aims to reduce SOC imbalances within a string by controlling the SOCs of the cells so that they become approximately equal. This can be achieved by dissipating energy from the cells of higher SOCs to shunt resistor (Fig. 2.16), or shuffling energy from the highest SOC cell to the lowest SOC cell (Fig. 2.17), or by incremental cell balancing through paired cells in stages [61–64].

The shunt resistor circuit in Fig. 2.16 is the simplest structure for cell balancing. When a cell's SOC is evaluated to be higher than others, its bypass circuit is turned on and the cell is discharged to reduce its SOC. The energy is lost as heat through the shunt resistor during the balancing. As a result, this cell balancing structure reduces battery efficiency. In contrast, the energy shuffling circuit in Fig. 2.17 will connect the cell with the highest SOC in the string to its balancing capacitor and charge the capacitor. The energy stored in the capacitor is then shuffled to the next

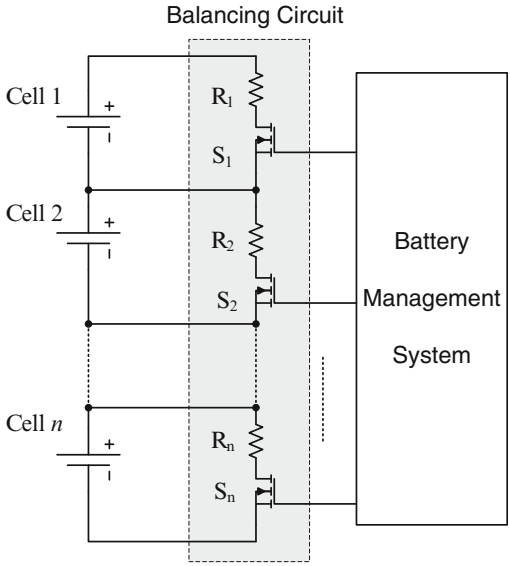

Fig. 2.16 Cell balancing through bypass resistors

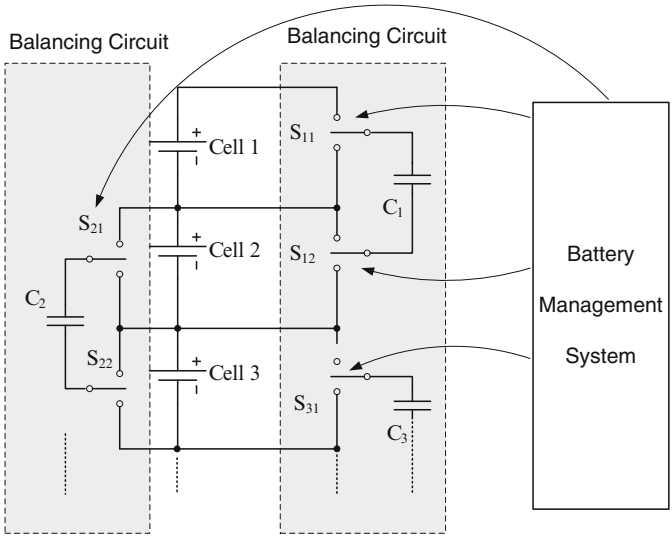

Fig. 2.17 Cell balancing through energy shuffling via capacitors

cell. This operation is repeated through the string to distribute gradually the energy from the cell with the highest SOC to other cells in the string. This balancing strategy increases battery efficiency, but incurs higher costs and longer time to finish the balancing process.

There are some principal design considerations and tradeoffs when cell balancing circuits are configured.

1. *Speed of Balancing*: It is always desirable to complete cell balancing as fast as possible. The downside of fast balancing is that the power rating of the balancing circuits will increase, causing higher loss and heat generation which in turn demands additional and costly thermal management. This also will make packaging more complicated.
2. *Energy Efficiency*: Dissipating energy to shunt resistors is a total energy loss, as shown in Fig. 2.16. As a result, it is only a viable choice for balancing of cells when the voltage deviations among cells are relatively small. However, such balancing circuits are very simple and sometimes the switching circuits and control can be integrated in ICs (integrated circuits). In contrast, energy shuffling can reduce significantly the energy loss, but requires additional energy storage components such as capacitors (or inductors) together with their power electronics and control functions, shown in Fig. 2.17. These increase costs and sizes with more sophisticated management systems.
3. *Voltage Balancing*: Although the intention of cell balancing is justifiably to equalize SOCs, for run-time implementation accurate SOC estimation and capacity determination are difficult. Consequently, many existing cell balancing systems are actually cell voltage balancing circuits. In other words, by comparing cell voltages, the balancing circuits try to equalize cell terminal voltages. This technology has fundamental drawbacks. Since terminal voltages are affected by cell impedances which are partially the reason for cell imbalance, equalizing terminal voltages will leave open-circuit voltages uneven when the cells are being charged or discharged at the same time. Since the open-circuit voltage is a better indicator of SOCs, terminal voltage balancing is always subject to imbalance on SOCs. In addition, the characteristic curves (terminal voltage vs. depth of charge/discharge) vary from cell to cell. When a cell ages, the cell voltage will be a poor indicator of its SOC. This is an acute problem for Li-ion batteries since their characteristic curves are quite flat in the normal operating ranges. This remains an active R&D area for manufacturers and research communities.

2.8 Battery Aggregation

The limited power capability of individual EVs prevents the direct participation of individual EVs in electricity markets. The integration of DER units using aggregation under the Virtual Power Plant (VPP) concept enables their visibility to the System Operator (SO) and so supports their market participation [65, 66]. In what follows, a classification of different VPP realizations is given and three VPP control architectures are introduced [67].

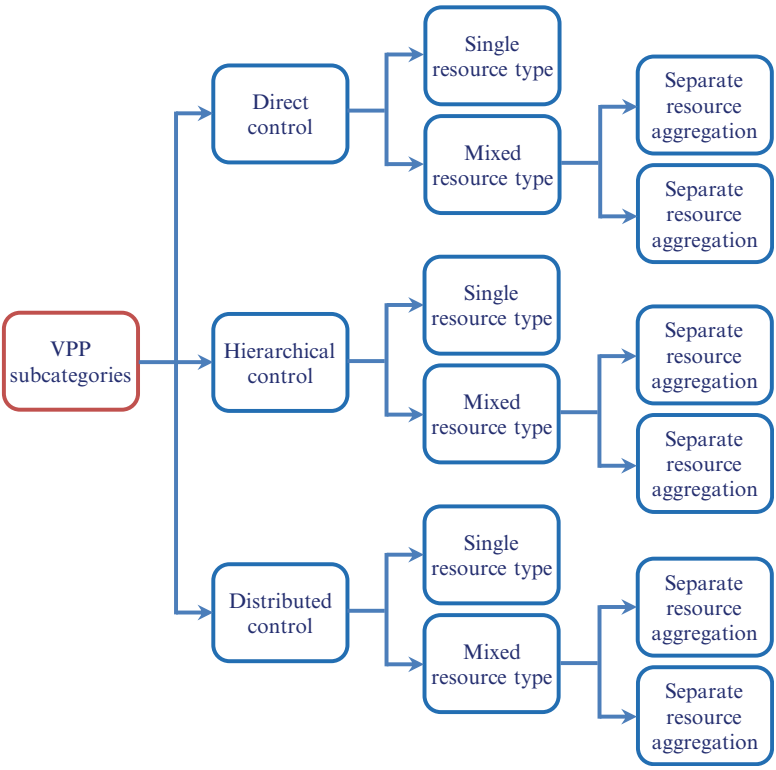

Fig. 2.18 Classification of different VPP realizations

2.8.1 Virtual Power Plant Realizations and Control

VPPs can be classified into several subcategories depending on the implemented control scheme and the aggregation type as presented in Fig. 2.18. The control approach used in VPPs may be direct, hierarchical, or distributed. The direct approach is based on a centralized control and decision-making concept. In the distributed control, on the other hand, the decisions for control of the VPP are made in a fully decentralized way. The hierarchical approach is the intermediate between direct and distributed control with some level of decision-making capability distributed in the VPP. In each VPP control approach, two subcategories of VPPs can be identified depending on the portfolio of the constituting resources. Contrary to single-resource-type VPPs, mixed-resource-type VPPs incorporate of a variety of resources. One approach to implementing these VPPs is to use a single module to handle all different resource categories. Alternatively, separate management modules for coordination of various types of resources may be considered. For example, an EV Management Module can be considered to specifically handle EV resources.

VPPs have so-called VPP Control Centers which are responsible for the optimal coordination of their resources and representing them as single entities to the market, DSOs, and TSOs. This unit needs updated information about the operation of VPP resources as well as the market status as inputs to its optimization functions. The use of information and communication technology (ICT) solutions allows the VPP Control Center to monitor and control the VPP resources in near real-time.

Within each VPP, it is possible that some entities are in charge of operating a number of individual resources. For example, so-called charging point managers (CPMs) may emerge as entities responsible for operating a number of EV charging points (CPs). In these cases, CPMs will represent their EVs to the VPP Control Center.

The CPs can be classified into three different categories based on their location. The CP location may be either in public areas with public access, private areas with private access, or private areas with public access. In each of these areas, the VPP Control Center may communicate with EVs in different ways. For example, the communication with EVs in private areas with private access may be realized through home energy management system (HEMS). An HEMS is an application that enables energy consumption management in a house taking into account the user preferences and allows interaction with the utility.

For the market participation, the VPP Control Center prepares bids and offers for the day-ahead and intraday markets based on the forecast about generation and demand of VPP resources. In real-time, using the measurement data from Smart Meters (SMs) and the updated input from market and the SO, the VPP Control Center decides and sends out adjustment requests to VPP resources.

2.8.1.1 Direct Control

In the direct control approach, the VPP Control Center is responsible for deciding and directly communicating the control requests with the individual VPP units or entities representing them. Within their limitations and based on preferences set by their owners, the resources will respond to the control requests received from the VPP Control Center.

Figure 2.19 summarizes the information flow paths in a direct VPP with a focus on EV integration. In this control approach, the VPP control center centrally takes care about the optimization of the operation of all individual VPP resources. The exceptions are cases where an entity such as a CPM is responsible for aggregating and representing a number of resources. Direct communication of the VPP Control Center with the VPP resources and the central decision-making process make this approach simple to implement.

2.8.1.2 Hierarchical Control

In a hierarchical control approach, intermediate aggregation functions are introduced for the VPP and aggregation takes place in different hierarchical layers.

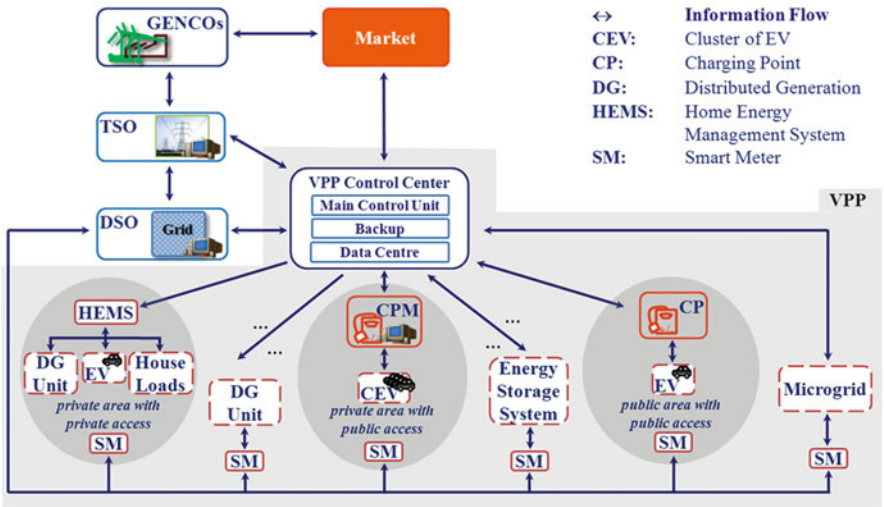

Fig. 2.19 Interaction between the VPP control center and the VPP resources, DSO, TSO, and market in the direct control approach

The EV Management Module (EVMM) is the module of the VPP which is responsible for the management of EVs under the VPP domain.

The EVMM prepares the EV market strategies as an input for the VPP Control Center, with the goal of minimizing EV battery charging cost and maximizing EV revenues. An EVMM comprises residential and commercial aggregation functions. This distinction enables the improvement of load predictions and identification of services to be offered from each group. Figure 2.20 shows the different levels of hierarchy.

2.8.1.3 Distributed Control

In a distributed control approach, a VPP Control Center does not have direct access to the DERs' operation but it can affect their behavior through price incentives. The VPP Control Center may follow different pricing strategies for consumption and generation. The core of the distributed concept is based on the ability of individual VPP entities to decide their optimal operational state. This requires that VPP entities have the adequate computational intelligence to obtain their private goals.

The information flow in the distributed VPP control is summarized is Fig. 2.21. In order to reduce the amount of information exchanged, an intermediate level of aggregation is implemented, referred to as VPP Local Aggregation (LA) functions, which is responsible for the coordinating of smaller geographical areas.

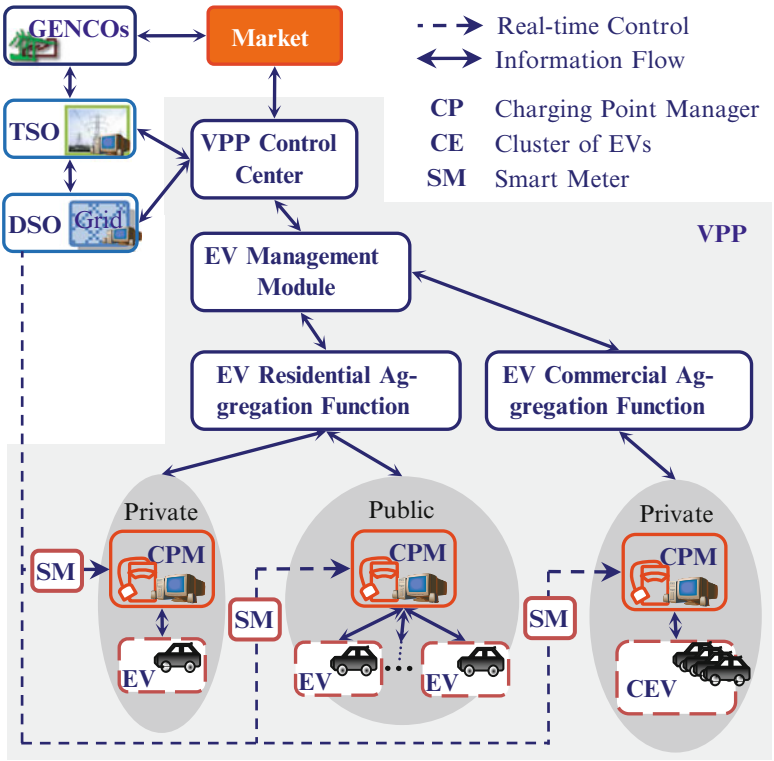

Fig. 2.20 Interaction between the VPP control center and the VPP resources, DSO, TSO, and the market in a hierarchical approach

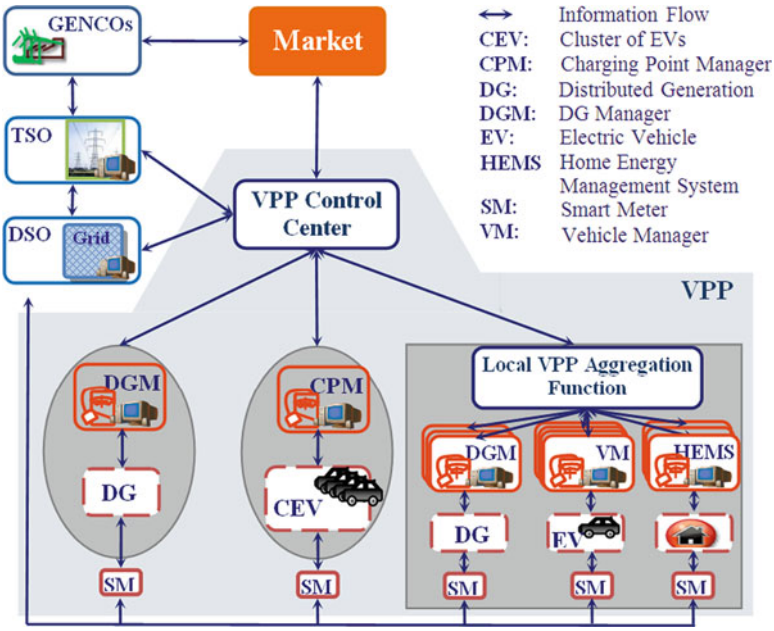

Fig. 2.21 Interaction between the VPP control center and the VPP resources, DSO, TSO, and the market in a distributed control approach

References

1. Howell D (2011) 2010 Annual progress report for energy storage R&D, Vehicle Technologies Program, Energy Efficiency and Renewable Energy. U.S. Department of Energy, Washington, DC
2. Boulanger AG, Chu AC, Maxx S, Waltz DL (2011) Vehicle electrification: status and issues. Proc IEEE 99(6):1116–1138
3. Xu X, Wang C, Liao G, Yeh CP, Stark W (2009) Development of a plug-in hybrid electric vehicle educational demonstration unit. In: Proceedings of 2009 North American power symposium, Starkville, MS, USA, 4–6 Oct 2009
4. Corrigan D, Masias A (2011) Batteries for electric and hybrid vehicles. In: Reddy TB (ed) Linden's handbook of batteries, 4th edn. McGraw Hill, New York
5. Ehsani M, Gao Y, Emadi A (2010) Modern electric, hybrid electric, and fuel cell vehicles: fundamentals, theory and design, 2nd edn. CRC, London
6. USABC (1996) Electric vehicle battery test procedures manual. http://avt.inl.gov/battery/pdf/usabc_manual_rev2.pdf
7. Coleman M, Hurley WG, Lee CK (2008) An improved battery characterization method using a two-pulse load test. IEEE Trans EC 23(2):708–713
8. Dhameja S (2002) Electric vehicle battery systems. Newnes, Boston
9. Pokrzywa J (2010) SAE Taipei: SAE ground vehicle standards SmartGrid. http://sae-taipei.org.tw/image/1283265726.pdf
10. Rocky Mountain Institute (2008) Smart garage Charrette pre-read v2.0. http://move.rmi.org/files/smartgarage/PreRead_v2_Core-1.pdf
11. http://www.peve.jp/e/hevkinzoku.html
12. Higashimoto K, Homma H, Uemura Y, Kawai H, Saibara S, Hirinaka K (2010) Automotive lithium-ion battery. Hitachi Hyoron 92(12):30–33
13. Moss PL, Au G, Plichta EJ, Zheng JP (2009) Investigation of solid electrolyte interface layer development during continuous cycling using ac impedance spectra and micro-structural analysis. J Power Sources 189:644–648
14. Strunz K, Louie H (2009) Cache energy control for storage: power system integration and education based on analogies derived from computer engineering. IEEE Trans Power Syst 24 (1):12–19
15. http://www.uscar.org/guest/article_view.php?articles_id=85
16. Ovshinsky SR, Fetcenko MA, Reichman B, Young K, Chao B, Im J (1997) US Patent 5,616,432
17. Ovshinsky SR, Corrigan D, Venkatesan S, Young R, Fierro C, Fetcenko MA (1994) US Patent 5,348,822
18. Esaka T, Sakagucji H, Kobayashi S (2004) Hydrogen storage in protpn-conductive perovskite-type oxide and their application to nickel-hydrogen batteries. Solid State Ionics 166 (3–4):351–357
19. Deng G, Chen Y, Tao M, Wu C, Shen X, Yang H, Liu M (2010) Electrochemical properties and hydrogen storage mechanism of perovskite-type oxide LaFeO3 as a negative electrode for Ni/MH batteries. Electrochim Acta 55 (3):1120–1124
20. http://www.khi.co.jp/english/gigacell/index.html
21. West JK, Higgins MP, Regalado J, George A (2009) US Patent Application 20090142655
22. http://www.arl.army.mil/www/pages/556/1109TFSHPCathodeLiIonBatteries.pdf
23. Sun Q, Li X, Wang Z, Ji Y (2009) Synthesis and electrochemical performance of 5V spinel LiNi0.5Mn1.5O4 prepared by solid-state reaction. Trans Nonferrous Met Soc Chin 19:176–181
24. Fetcenko MA (2011) In: Presentation in Batteries 2011, Cannes Mandelieu, France, 20–28 Sep 2011
25. Mitchell RR, Gallany BM, Thompson CV, Yang S (2011) All-carbon-nanofiber electrodes for high-energy, rechargeable Li-O_2 batteries. Energy Environ Sci 4:2952–2958

26. Dubarry M, Vuillaume N, Liaw BY (2009) From single cell model to battery pack simulation for Li-ion batteries. J Power Sources 186:500–507
27. Song L, Evans JW (2000) Electrochemical-thermal model of lithium polymer batteries. J Electrochem Soc 147:2086–2095
28. Min C, Gabriel AR (2006) Accurate electrical battery model capable of predicting runtime and I–V performance. IEEE Trans Energy Conversion 21(2):504–511
29. Gomadam PM, Weidner JW, Dougal RA, White RE (2002) Mathematical modeling of lithium-ion and nickel battery systems. J Power Sources 110(2):267–24
30. Dennis DW, Battaglia VS, Belanger A (2002) Electrochemical modeling of lithium polymer batteries. J Power Source 110(2):310–320
31. Newman J, Thomas KE, Hafezi H, Wheeler DR (2003) Modeling of lithium-ion batteries. J Power Sources 119–121:838–843
32. Rynkiewicz R (1999) Discharge and charge modeling of lead acid batteries. Proc Appl Power Electron Conf Expo 2:707–710
33. Rakhmatov D, Vrudhula S, Wallach DA (2003) A model for battery lifetime analysis for organizing applications on a pocket computer. IEEE Trans VLSI Syst 11(6):1019–1030
34. Rong P, Pedram M (2003) An analytical model for predicting the remaining battery capacity of lithium-ion batteries. In: Proceedings of design, automation, and test in Europe conference and exhibition, pp 1148–1149
35. Pascoe PE, Anbuky AH (2004) VRLA battery discharge reserve time estimation. IEEE Trans Power Electron 19(6):1515–1522
36. Salameh ZM, Casacca MA, Lynch WA (1992) A mathematical model for lead-acid batteries. IEEE Trans Energy Convers 7(1):93–98
37. Valvo M, Wicks FE, Robertson D, Rudin S (1996) Development and application of an improved equivalent circuit model of a lead acid battery. Proc Energy Convers Eng Conf 2:1159–1163
38. Ceraolo M (2000) New dynamical models of lead-acid batteries. IEEE Trans Power Syst 15(4):1184–1190
39. Barsali S, Ceraolo M (2002) Dynamical models of lead-acid batteries: implementation issues. IEEE Trans Energy Convers 17(1):16–23
40. Schweighofer B, Raab KM, Brasseur G (2003) Modeling of high power automotive batteries by the use of an automated test system. IEEE Trans Instrum Meas 52(4):1087–1091
41. Gao L, Liu S, Dougal RA (2002) Dynamic lithium-ion battery model for system simulation. IEEE Trans Compon Packag Technol 25(3):495–505
42. Baudry P, Neri M, Gueguen M, Lonchampt G (1995) Electro-thermal modeling of polymer lithium batteries for starting period and pulse power. J Power Sources 54(2):393–396
43. Abu-Sharkh S, Doerffel D (2004) Rapid test and non-linear model characterization of solid-state lithium-ion batteries. J Power Sources 130:266–274
44. Bard A, Faulkner L (2001) Electrochemical methods: fundamentals and applications, 2nd edn. Wiley, New York
45. Doyle M, Newman J, Gozdz AS, Schmutz CN, Tarascon JM (1996) Comparison of modelling predictions with experimental data from plastic lithium ion cells. J Electrochem Soc 143:1890
46. Tremblay O, Dessaint L-A (2009) Experimental validation of a battery dynamic model for EV applications. In: EVS24 international battery, hybrid and fuel cell electric vehicle symposium, Stavanger, Norway, 13–16 May 2009, World Electric Vehicle J 3
47. Johnson VH (2001) Battery performance models in ADVISOR. J Power Sources 110:321–329
48. Wang C, Nehrir MH, Shaw SR (2005) Dynamic models and model validation for PEM fuel cells using electrical circuits. IEEE Trans Energy Convers 20(2):442–451
49. Barbier C, Meyer H, Nogarede B, Bensaoud S (1994) A battery state of charge indicator for electric vehicle. In: Proceedings of the international conference of the institution of mechanical engineers, automotive electronics, London, UK, 17–19 May 1994, pp 29–34
50. Dai HF, Wei XZ, Sun ZC (2006) Online SOC estimation of high-power lithium-ion batteries used on HEVs. In: Proceedings of IEEE ICVES 2006, pp 342–347

51. Giglioli R, Pelacchi P, Raugi M, Zini G (1988) A state of charge observer for lead-acid batteries. Energia Elettrica 65(1):27–33
52. Plett G (2004) Extended Kalman filtering for battery management systems of LiPB-based HEV battery packs. Part 1: Background. J Power Sources 134(2):252–261
53. Rodrigues S, Munichandraiah N, Shukla A (2000) A review of state-of-charge indication of batteries by means of ac impedance measurements. J Power Sources 87(1/2):12–20
54. Kuo BC (1995) Digital control systems, 2nd edn. Oxford University Press, Oxford
55. Barsoukov E, Kim J, Yoon C, Lee H (1999) Universal battery parameterization to yield a non-linear equivalent circuit valid for battery simulation at arbitrary load. J Power Sources 83(1/2):61–70
56. Plett G (2004) Extended Kalman filtering for battery management systems of LiPB-based HEV battery packs. Part 2. Modeling and identification. J Power Sources 134(2):262–276
57. Takano K, Nozaki K, Saito Y, Negishi A, Kato K, Yamaguchi Y (2000) Simulation study of electrical dynamic characteristics of lithium-ion battery. J Power Sources 90(2):214.223
58. Ljung L (1987) System identification: theory for the user. Prentice-Hall, Englewood Cliffs, NJ
59. Wang LY, Yin G, J-f Z, Zhao Y (2010) System identification with quantized observations. Birkhauser, Boston, MA. ISBN 978-0-8176-4955-5
60. Sitterly M, Wang LY, Yin G, Wang C (2011) Enhanced identification of battery models for real-time battery management. IEEE Trans Sustain Energy 2:300–308
61. Moore SW, Schneider P (2001) A review of cell equalization methods for lithium ion and lithium polymer battery systems. SAE Publication, Troy, MI
62. Linden D, Reddy T (2001) Handbook of batteries, 3rd edn. McGraw Hill, New York
63. Kutkut NH, Wiegman HLN, Divan DM, Novotny DW (1999) Design considerations for charge equalization of an electric vehicle battery system. IEEE Trans Ind Appl 35:28–35
64. Tang M, Stuart T (2000) Selective buck-boost equalizer for series battery packs. IEEE Trans Aerospace Electron Syst 36:201–211
65. Pudjianto D, Ramsay C, Strbac G (2008) Microgrids and virtual power plants: concepts to support the integration of distributed energy resources. Proc Inst Mech Eng A J Power Energy 222(7):731–741
66. Karfopoulos E, Tsikalakis A, Karagiorgis G, Dimeas A, Christodoulou C, Tomtsi T, Hatziargyriou N (2009) Description of the off-line simulations. Task and results presentation. EUDEEP Project WP4&5, Task Force 3, Jan 2009
67. Raab AF, Ferdowsi M, Karfopoulos E, Grau Unda I, Skarvelis-Kazakos S, Papado poulos P, Abbasi E, Cipcigan LM, Jenkins N, Hatziargyriou N, Strunz K (2011) Virtual power plant control concepts with electric vehicles. In: 16th International conference on intelligent system applications to power systems, Hersonissos, Greece, Sep 2011
68. http://www.mathworks.com/help/toolbox/physmod/powersys/ref/battery.html
69. Lezhang L, Wang LY, Chen Z, Wang C, Lin F, Wang H (2012) Integrated system identification and state-of-charge estimation of battery systems. IEEE Trans Energy Conversion (In press)

http://www.springer.com/978-1-4614-0133-9

Electric Vehicle Integration into Modern Power Networks
Garcia-Valle, R.; Peças Lopes, J.A. (Eds.)
2013, XI, 325 p. 202 illus., 134 illus. in color., Hardcover
ISBN: 978-1-4614-0133-9